



1 Precipitation-fire-functional interactions control biomass stocks and
2 carbon exchanges across the world's largest savanna

3

4 Mathew Williams^{1,2,*}, David T Milodowski^{1,2}, T Luke Smallman^{1,2}, Kyle G Dexter¹, Gabi C Hegerl¹, Iain
5 M McNicol¹, Michael O'Sullivan³, Carla M Roesch¹, Casey M Ryan^{1,2}, Stephen Sitch³ and Aude Valade⁴

6

7 ¹ School of GeoSciences, University of Edinburgh, EH9 3FF, UK

8 ² National Centre for Earth Observation, University of Edinburgh, EH9 3FF, UK

9 ³ Faculty of Environment, Science and Economy, University of Exeter, EX4 4QF, UK

10 ⁴ Eco&Sols, Univ Montpellier, CIRAD, INRAE, Institut Agro, IRD, Montpellier, France

11

12 * Corresponding author: mat.williams@ed.ac.uk

13



1

2 1 Abstract

3 Southern African woodlands (SAW) are the world's largest savanna, covering ~ 3 M km², but their carbon
4 balance, and its interactions with climate and disturbance are poorly understood. Here we address three
5 issues that hinder regional efforts to address international climate agreements: producing a state-of-the-art
6 C budget of SAW region; diagnosing C cycle functional variation and interactions with climate and fire
7 across SAW; and evaluating SAW C cycle representation in land surface models (LSMs). Using 1506
8 independent 0.5° pixel model calibrations, each constrained with local earth observation time series of
9 woody carbon stocks (C_{wood}) and leaf area, we produce a regional SAW C analysis (2006-2017). The
10 regional net biome production is neutral, 0.0 Mg C ha⁻¹ yr⁻¹ (95% Confidence Interval $-1.7 - 1.6$), with fire
11 emissions contributing ~ 1.0 Mg C ha⁻¹ yr⁻¹ (95% CI 0.4-2.5). Fire-related mortality driving fluxes from total
12 coarse wood carbon (C_{wood}) to dead organic matter likely exceeds both fire-related emissions from C_{wood} to
13 atmosphere and non-fire C_{wood} mortality. The emergent spatial variation in biogenic fluxes and C pools is
14 strongly correlated with mean annual precipitation and burned area. But there are multiple, potentially
15 confounding, causal pathways through which variation in environmental drivers impacts spatial distribution
16 of C stocks and fluxes, mediated by spatial variations in functional parameters like allocation, wood lifespan
17 and fire resilience. Greater C_{wood} in wetter areas is caused by positive precipitation effects on net primary
18 production and on parameters for wood lifespan, but is damped by a negative effect with rising precipitation
19 increasing fire-related mortality. Compared to this analysis, LSMs showed marked differences in spatial
20 distributions and magnitudes of C stocks and fire emissions. The current generation of LSMs represent
21 savanna as a single plant functional type, missing important spatial functional variations identified here.
22 Patterns of biomass and C cycling across the region are the outcome of climate controls on production, and
23 vegetation-fire interactions which determine residence times, linked to spatial variations in key ecosystem
24 functional characteristics.

25

26 Key words: SAW, Southern Africa, LAI, land surface models, fire, vegetation carbon



1 2 Introduction

2 Tropical savannas, dominated by trees and grasses, cover 40% of the vegetated tropics (Pennington et al.,
3 2018) including 2.3-3.1 M km² in southern Africa (Ribeiro et al., 2020; Ryan et al., 2016). Savanna C stocks
4 and net C fluxes are substantial in the global carbon cycle (Sitch et al., 2015), but with major geographical
5 variations. Spatially there is a strong coupling between precipitation and tree cover across African savanna,
6 particularly where annual precipitation is < 800 mm (Sankaran et al., 2005). The presence of substantial,
7 dry fuel loads means that disturbance from fire is common during the dry season (Andela et al., 2017). Fire
8 influences decadal C sinks through combustion related emissions (van der Werf et al., 2017) and
9 disturbance impacts on both vegetation growth rates (Yin et al., 2020) and tree mortality (Levick et al.,
10 2015). Overall, the interactions of climate and disturbance, particularly from fire, generate dynamic
11 conditions for C stocks and fluxes across tropical savannas and woodlands (Archibald et al., 2013; Lehmann
12 et al., 2014), which are poorly mapped and understood.

13

14 Southern African woodlands (SAW) are the dominant land cover in the dry tropics of southern Africa
15 (Campbell, 1996), and form the world's largest savanna (Mistry, 2014; Ryan et al., 2016), covering much
16 of Tanzania, Mozambique, Zambia, Zimbabwe, Malawi, Angola and southern DRC. The woodlands of this
17 region are phylogenetically distinct from other tropical savannas (Dexter et al., 2015) and have
18 biogeochemical and fire patterns (Alvarado et al., 2020) that are linked to unique functional traits (Osborne
19 et al., 2018). These woodlands have long been subjected to, and thus are highly adapted to, disturbance by
20 people, fire (generally set by people), and herbivores (Chidumayo, 2002; Chidumayo, 2004). Overall, the
21 woodland C cycle is often non-steady-state, and anthropogenic change is strengthening this tendency (Ryan
22 et al., 2016). Fire impacts on the C cycle and vegetation C stocks are linked to wet seasons moist enough
23 for biological production to generate fuel load, and dry seasons intense enough to dry fuel for destructive
24 fires. Wetter areas of the SAW region may have biomass stimulated by rising production but limited by
25 rising mortality from fire.

26

27 A complete ecosystem C cycle analysis for the SAW region, that spans climatic gradients, resolves process
28 interactions between climate, fire and the ecological functioning of C cycling, does not currently exist.
29 There are knowledge gaps both on biosphere-atmosphere exchanges and on internal ecosystem processing
30 of C. Deriving dynamics of C requires quantification and linkage of relevant processes controlling the
31 biosphere-atmosphere exchange of C, its allocation or transfer to different C pools, and the turnover of
32 these pools. Eddy flux data are scarce and short term in this region (Merbold et al., 2009). As a result, the
33 net biome exchange (NBE) of CO₂ and its components (e.g. gross primary production (GPP), ecosystem



1 respiration (R_{eco}), fire emissions (E_{Fire}) remain poorly quantified (Ciais et al., 2011; Ernst et al., 2024).
2 Internal C processes, particularly mortality or turnover of key pools (linked to mean residence time, MRT),
3 are critical for determination of C balance but poorly quantified (Friend et al., 2014; Smallman et al., 2021).
4 The MRT is the ratio of C pool size to the total losses from that pool per unit time. In savanna, MRT is
5 sensitive to both external factors like burning and to internal ecosystem properties. External factors like
6 burning are likely to shorten residence times, but vegetation may adapt to burning with increased tissue
7 resilience to fire. Plant tissue (wood, foliage) lifespans may vary spatially, for instance with climate.
8
9 These C cycle knowledge gaps hinder national efforts to manage savanna carbon stores to meet international
10 actions like the Paris Agreement of the UNFCCC. Also, these gaps weaken model projections of trajectories
11 of C for this region under climate change. Simulation models typically represent tropical woodlands across
12 the globe using a single ‘plant functional type’ (PFT), with PFT-specific parameters which may lead to
13 biased outcomes (Bloom et al., 2016). The functional differences within the savanna biome (Lehmann et
14 al., 2014; Moncrieff et al., 2014) mean that region-specific carbon cycle estimates linked to locally valid
15 functional characteristics are required. Even within the SAW region, we expect to find biological variation
16 and gradients in functional characteristics (Osborne et al., 2018). Understanding this variation and links to
17 the environment can underpin more robust knowledge. This knowledge can improve representation and
18 therefore forecasts from land surface models, for instance those used to study trends in the land carbon
19 cycle, such as the Trendy experiment (Sitch et al., 2015).
20
21 Insights into SAW C cycling are accumulating through intensive studies and extensive observations.
22 Researchers have developed robust methods for woodland inventory and landscape sampling (SEOSAW
23 partnership, 2021). Chronosequence studies have documented the biomass recovery rates of these
24 ecosystems post-disturbance (Chidumayo, 2004; Chidumayo, 2013; Kalaba et al., 2013; Gonçalves et al.,
25 2017) to provide insights into annual to decadal dynamics. Earth observations (EO) of vegetation greening
26 (changes in leaf area index, LAI) have been found reliable against *in situ* data on canopy phenology (Ryan
27 et al., 2014; Ryan et al., 2017) and hence can map potential for photosynthesis in time and space. Radar
28 remote sensing has been identified as an effective tool for mapping biomass and its changes over these
29 landscapes (Ryan et al., 2012; Mitchard et al., 2009). These actions have developed the first regional
30 analyses for biomass in space and time (McNicol et al., 2018; McNicol et al., 2023). Long term observations
31 from satellites track the burned area across these landscapes (Chuvieco et al., 2019). These multiple new
32 analyses of the SAW region provide an opportunity to generate a more robust assessment of the C cycle
33 from local to regional scales. Mechanistic models calibrated with these data can provide a complete,
34 constrained, and probabilistic quantification of the carbon cycle and its processes.



1

2 In the present study, we combine new spatial data products with a model-data fusion system (CARDAMOM
3 (Bloom and Williams, 2015)), to create the most comprehensive diagnostic analysis to date of the CO₂-C
4 cycle of the SAW region in southern Africa. We use this analysis to address questions about key controlling
5 processes on the dynamics of major C pools, and their variation with climate and fire disturbance across
6 the region for 2006-2017. We further characterise net CO₂ exchanges resulting from different driving
7 factors and variations in plant processes, including allocation and mortality. Net ecosystem exchange (NEE
8 = R_{eco} – GPP; sink has a negative sign) is purely biogenic, i.e. biological processes driven by atmospheric
9 conditions. Net biome production (NBP) includes human-driven emissions from prescribed factors such as
10 fire and land use removals (NBP = – NEE – fire emissions – biomass removals by external factors; sink has
11 a positive sign). Specifically, this study generates a full C cycle analysis and asks the following research
12 questions (RQ):

- 13 1. How do fluxes and resulting net exchanges of CO₂ vary across the SAW region and covary with
14 climate, fire, and functional characteristics?
- 15 2. How do carbon stocks and their longevity covary with climate, fire, and functional characteristics?
- 16 3. How does data-constrained analysis of ecosystem C cycling compare to Trendy land surface model
17 estimates for the region?

18

19 For RQ1 we hypothesise that biogenic fluxes (GPP, R_{eco}) will be determined by a positive relationship with
20 precipitation, the dominant control on biological metabolism in SAW (Campbell, 1996). We hypothesise
21 that NBP across SAW will be determined by a negative relationship with burned area, through fire
22 emissions (E_{Fire}). For RQ2 we hypothesise that C stocks in total coarse wood C (C_{wood}) will be positively
23 correlated with, and their distribution determined by, precipitation. But we hypothesise there will be
24 mediating effects from variations in functional characteristics such as wood lifespan and fire resilience,
25 evidenced by broad scale gradients in these ecosystem functional characteristics. For RQ3 we hypothesise
26 that comparisons of land surface models from Trendy with CARDAMOM analyses will be more consistent
27 in biosphere-atmosphere fluxes than in stock estimates, because of the challenge of calibrating modelled
28 stocks to observations (Fawcett et al., 2022).

29 The novelty of this research is threefold. The regional C budget produced here is state-of-the-art due to its
30 consistency with locally calibrated estimates of woody biomass dynamics from earth observation. Causal
31 inference approaches disentangle emergent spatial patterns in C dynamics and ecosystem functional
32 characteristics, providing new biogeographical understanding of ecological functioning and diversity. The
33 spatially detailed model calibration builds an emergent map of process and C cycle variation that allows
34 resolution of within biome patterns, enhancing assessment of LSMs.



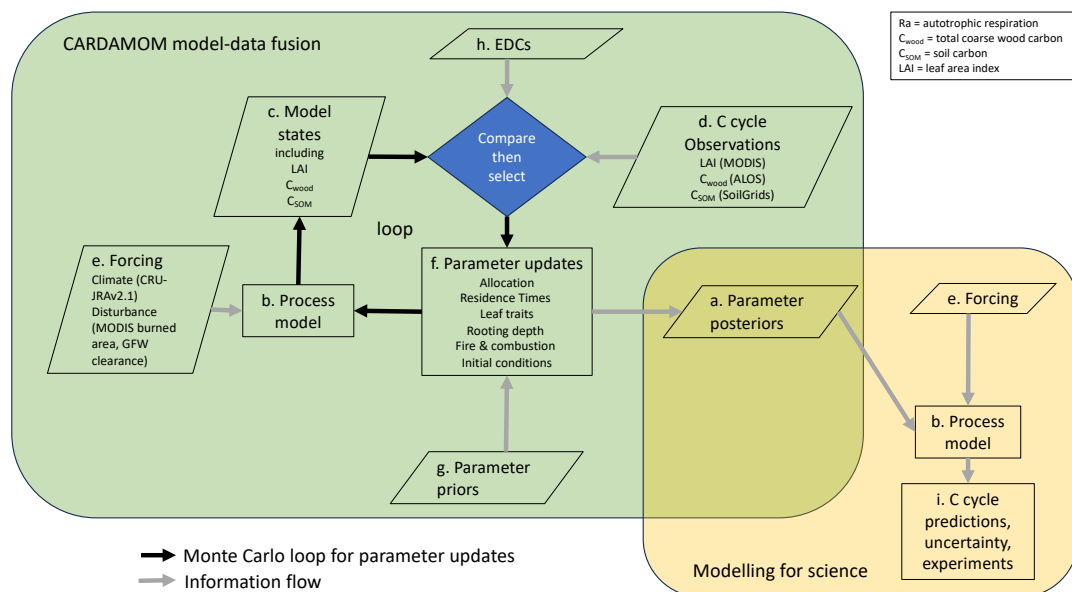
1

2 **3 Methods**

3 Multiple EO products of C stocks and LAI, and a soil C map, are combined into a pixel-by-pixel regional
 4 analysis, through assimilation with an intermediate complexity biophysical ecosystem model (Bloom and
 5 Williams, 2015) that is calibrated over the area of interest (Figure 1) with local climate, fire and forest
 6 clearance forcing data. The result is a rigorous, probabilistic C cycle assessment, including GPP, NBP,
 7 allocation to tissues, pool sizes, ecosystem processes, fire emissions, fire mortality and non-fire mortality.
 8 Calibrated parameters and C cycle assessments are produced independently for each of the 1506 model
 9 pixels at 0.5° spatial and monthly temporal resolution for a 12-year period (2006-2017 inclusive). The study
 10 domain comprises all of Tanzania, Mozambique, Zambia, Zimbabwe, Malawi, Angola and southern
 11 Democratic Republic of Congo (DRC) and covers 4.5 M km², including miombo woodland and a mix of
 12 other woodland and savanna types and land uses (SEOSAW partnership, 2021; Godlee et al., 2021).
 13 Statistical analysis then relates the spatially independent, data-consistent analytical outputs of each pixel to
 14 climate, fire/human disturbance and to outputs of LSMs to address the research questions.

15

16



17

18

19 Figure 1. Schematic of the CARDAMOM methodology (green box) and modelling process (yellow box).

20 The Carbon Data Model Framework (CARDAMOM) generates parameter estimates with uncertainty (a)



1 for a process model (b). Independent estimates are made for each location (pixel) in the analysis. Parameter
2 estimates are constrained to ensure that specific model state variable predictions (c) match independent
3 observations for those variables at that location (d). Model predictions are made using local forcing data on
4 climate and disturbance (e). The model has 32 parameters (f) that govern biological processes, fire impacts
5 and include 7 initial conditions, with priors provided for each (g). A Monte Carlo process explores
6 parameter space defined by the priors, comparing model estimates (c) with observations (d), and using
7 ecological and dynamical constraints (EDCs, h) to inform selection (accept/reject) of parameter
8 combinations. Once parameter posterior ensembles are generated for each pixel (a), then a separate
9 modelling process uses these parameters to generate ensemble C cycle estimates for each pixel (i) using the
10 model (b) and specified forcing (e).

11

12

13 **3.1 Environmental data**

14 *3.1.1 Biomass, LAI time series and soil C data for calibration*

15 25 m resolution L-band radar data from ALOS-PALSAR were used to estimate aboveground woody carbon
16 (AGC), based on a calibration with field estimates (McNicol et al., 2018). We used a scalar linking above
17 and belowground wood C stocks ($C_{\text{wood}} = 1.42 \times \text{AGC}$ (Ryan et al., 2011)) to prepare four annual 0.5° maps
18 of C_{wood} for the 4-year period 2007-2010 based on higher resolution data from McNicol et al. (2018).
19 Uncertainty in the biomass observations (2.5 tC ha^{-1}) was estimated based on a local characterisation of
20 bias in retrieved biomass (McNicol et al., 2018).

21 MODIS EO (Myneni et al., 2021) product number MCD15A2H.061 provided 8-day composite information
22 on LAI (2006-2017) aggregated to months. Prior information on soil carbon stocks to a depth of 1.0 m were
23 drawn from the SoilGrids2 database (250 m resolution), a machine-learning based interpolation of field
24 inventories (Hengl et al., 2017). All data were aggregated to the 0.5° model spatial grid resolution. LAI and
25 soil carbon estimates were provided with a corresponding uncertainty estimate from their respective
26 products. The assimilation makes uses of LAI data available for all months of the analysis ($n=144$), biomass
27 data for four of the 12 years ($n=4$), and soil C data as a single value applied to its initial status ($n=1$).

28 *3.1.2 Disturbance and burned area observations for driving analyses*

29 MODIS product number MCD64A1.061 provided monthly, 500 x 500 m burned area data (Giglio et al.,
30 2018). Tree cover loss is imposed as a fractional removal of biomass, derived from the 30-m resolution
31 Global Forest Watch data on area disturbed (Hansen et al., 2013). Both data sets were aggregated to the
32 model 0.5° spatial grid and monthly resolution. Land use change or vegetation transition was not included
33 in the dynamics of the modelled ecosystem.



1 *3.1.3 Woody biomass chrono-sequences for model validation*

2 Chronosequence data provided estimates of the accumulation rate of woody biomass for two areas in the
3 SAW region. At N'hambita, Mozambique, we generated estimates of biomass from 28 plots each of 0.125
4 ha, with age since abandonment ranging from 2-30 years (Williams et al., 2008). At Kilwa District,
5 Tanzania, we used estimates from 55 plots each of 0.2 ha, with age-since-abandonment of 2-47 years
6 (McNicol et al., 2015).

7 *3.1.4 Meteorological and soil physics data for model forcing and soil parameters*

8 CARDAMOM meteorological drivers were extracted from the CRU-JRAv2.1 dataset, a 6-hourly 0.5°
9 dataset of precipitation using the Japanese Reanalysis product (see (Harris, 2019)) and aggregated to
10 monthly resolutions (Figure S 1). Soil sand/clay fractions required for estimating soil hydraulic properties
11 for input to the ecosystem model in CARDAMOM are extracted from the SoilGrids2 dataset.
12

13 **3.2 Modelling the carbon cycle**

14 *3.2.1 Terrestrial Ecosystem Model*

15 An intermediate complexity ecosystem model, DALEC-4 (Williams et al., 2005), simulated carbon stored
16 in both live biomass (labile, foliage, fine roots and total coarse wood which includes stems, branches, and
17 coarse roots) and dead organic matter (a litter pool, and a Soil Organic Matter (SOM) pool that includes
18 coarse wood debris). The model simulates C flows (allocation and turnover/mortality) between pools and
19 with the atmosphere (photosynthesis and respiration) and requires 25 parameters and 7 initial conditions
20 (Table 1). Processes are sensitive to climate drivers, and pools are sensitive to disturbance drivers (fire and
21 other biomass removal). Photosynthetic uptake (GPP) is estimated by the Aggregated Canopy Model,
22 ACM2 (Smallman and Williams, 2019), as a function of temperature, solar radiation, atmospheric CO₂,
23 precipitation and LAI (LAI is simulated by DALEC). Water supply to the canopy is generated by a coupled
24 water cycle model which estimates ecosystem water stock and accessibility as a function of precipitation,
25 soil texture and wood and root C stocks. Autotrophic respiration (R_a) is estimated as a fixed fraction of
26 GPP. Net primary production ($NPP = GPP - R_a$) is allocated using fixed fractions to live pools.
27 Heterotrophic respiration of litter and soil carbon (R_h) is estimated as a function of carbon stock, a turnover
28 rate and a temperature coefficient. Ecosystem respiration (R_{eco}) is the sum of R_a and R_h . Canopy phenology
29 is simulated by a model with pixel-specific fixed times each year for budburst and leaf senescence. Bud
30 burst leads to allocation of C from the labile to foliar pool. Leaf senescence initiates turnover of C from the
31 foliar pool. There is no explicit separation of tree and grass components in the model.

32



Parameter	Prior low	Prior high	Units	Posterior to prior ratio	Parameter type
Decomposition rate	0.00001	0.01	d ⁻¹	0.88	res
Fraction of GPP respired	0.2	0.8	fraction	0.61	all
Fraction of NPP to foliage	0.1	0.5	fraction	0.63	all
Fraction of NPP after labile allocation to roots	0.1	0.8	fraction	0.83	all
Leaf Lifespan	1.001	6	y	0.09	fol
TOR wood	0.000009	0.001	d ⁻¹	0.53	res
TOR roots	0.001368	0.02	d ⁻¹	0.90	res
TOR litter	0.0001141	0.02	d ⁻¹ at 0°C	0.94	res
TOR SOM	0.000001368	0.00009126	d ⁻¹ at 0°C	0.82	res
temperature factor, Q10	0.019	0.08	-	0.93	res
Canopy efficiency	10	100	gCm ⁻² d ⁻¹	0.23	fol
Leaf onset day	365.25	1461	Day of year	0.12	fol
Fraction of NPP after leaf allocation to C _{lab}	0.01	0.5	fraction	0.55	all
C _{lab} release period	10	100	d	0.68	fol
Leaf fall onset day	365.25	1461	Day of year	0.03	fol
Leaf fall period	20	150	d	0.48	fol
LCA (leaf C per area)	20	180	gCm ⁻²	0.75	fol
IC C _{lab}	1	2000	gCm ⁻²	0.03	init
IC C _{fol}	1	2000	gCm ⁻²	0.13	init
IC C _{root}	1	2000	gCm ⁻²	0.20	init
IC C _{wood}	1	30000	gCm ⁻²	0.02	init
IC C _{litter}	1	2000	gCm ⁻²	0.13	init
IC C _{SOM}	200	250000	gCm ⁻²	0.03	init
IC soil water as fraction of field capacity	0.5	1	fraction	0.84	init
Fraction of C _{wood} which is coarse root	0.15	0.5	fraction	0.94	root
Coarse root biomass to reach 50 % of max rooting depth	100	2500	g m ⁻²	0.82	root
Max rooting depth	0.35	20	m	0.83	root
Biomass resilience to fire	0.01	0.99	fraction	0.62	fire
Combustion completeness for foliage	0.01	0.99	fraction	0.73	fire
Combustion completeness for root and wood	0.01	0.99	fraction	0.24	fire
Combustion completeness for soil	0.01	0.1	fraction	0.58	fire
Combustion completeness for litter	0.01	0.99	fraction	0.90	fire



1 Table 1 Parameters for the DALEC model, showing their prior and posterior values for a selected
2 location, units, and the ratio of the posterior 95% confidence interval to the prior range. Parameters are
3 categorised according to their role in C dynamics as follows: Allocation (all), residence times (res), foliar
4 traits (fol), rooting depth (root), fire and combustion (fire) and initial conditions (init). TOR is turnover rate.
5 IC is initial condition. C_{lab} is labile C pool that supports leaf flushing.

6
7 Fire emissions are determined from the fraction of each pixel burned multiplied by a combustion fraction
8 parameter from Exbrayat et al. (2018). Specific combustion parameters are applied for each C pool. Of the
9 non-combusted vegetation pools in the burned fraction, fire mortality moves a fraction of C to the SOM
10 pool, using a resilience parameter common to all tissues. The SOM pool is assumed to include coarse woody
11 debris (CWD), and simulated fire emissions from the SOM pool therefore include the contribution from
12 CWD. A fraction of the litter pool is converted to SOM because of fire. For biomass removals linked to
13 land use, C losses are determined by the fraction of each pixel deforested as identified by GFW forcing
14 data, with all foliage C transferred to litter pools, and 80% of aboveground wood biomass removed from
15 the ecosystem (i.e. human extraction). Other pools are not deemed affected by this disturbance.

16

17 *3.2.2 Calibration using model-data fusion*

18 CARDAMOM is a model-data fusion framework (MDF) which combines local observations, their
19 uncertainties and ecological knowledge of the terrestrial C cycle to calibrate DALEC parameters
20 probabilistically. CARDAMOM uses a Bayesian approach within an Adaptive-Proposal Markov Chain
21 Monte Carlo (AP-MCMC) algorithm to retrieve ensembles of local parameters for each 0.5° pixel,
22 consistent with local observations, uncertainties, climate and disturbance forcing, and ecological theory
23 embedded in DALEC's structure (Bloom et al., 2016).

24 All DALEC parameters have a specified prior range to guide calibration (Table 1). Specific prior estimates
25 (i.e. mean + uncertainty) are provided based on literature studies for (i) the fraction of GPP allocated to R_a
26 (R_a : $GPP = 0.46 \pm 0.12$ (Waring et al., 1998; Collalti and Prentice, 2019)) and (ii) the canopy photosynthetic
27 efficiency ($C_{eff} = 21.1 \pm 8.5$ (Kattge et al., 2011)). CARDAMOM imposes ecological realism, or common
28 sense, on parameter retrievals using ecological and dynamic constraints, EDCs. EDCs set the likelihood of
29 a given parameter proposal to 0 if none of the conditions defined by the EDCs are met. The EDCs are
30 intended to prevent three kinds of ecologically inconsistent parameter proposals: 1) unrealistic
31 combinations, e.g. to ensure that turnover of fine roots is faster than for wood (in the absence of
32 disturbance), 2) maintaining emergent ecosystem ratios within observed ranges, e.g. fine root to foliar ratio,
33 3) preventing inappropriate carbon stock dynamics such as exponential carbon stock changes on short time



1 scales outside disturbance/fire. The resultant DALEC parameter uncertainty encompasses the combined
2 uncertainties of the observational constraints, parameter priors, the prior ranges and the plausible ecological
3 parameter space as defined by the EDCs.

4 *3.2.3 Validation against independent regional products*

5 Once calibrated probabilistically at each pixel, DALEC is then run using the same forcing data to generate
6 local ensembles of C cycle estimates (Figure 1). The first stage of validation tests the calibration process
7 by evaluating the simulated LAI, C_{wood} and soil C against the assimilated data for these variables to test for
8 an unbiased estimate and for spatial coherence (random error across pixels) for each variable. The second
9 stage of tests is to evaluate the CARDAMOM analyses against other regional products. For NBE the
10 reanalyses are compared against an ensemble of Carbon Tracker Europe (CTE) estimates (Koren, 2020);
11 for GPP against the combined estimates from FluxCOM (Jung et al., 2020), Copernicus (Fuster et al., 2020)
12 and FluxSatv2 (Joiner and Yoshida, 2021); and for fire emissions against the combined estimates of
13 GFEDv4.1s (van der Werf et al., 2017) and GFAS (Kaiser et al., 2012). The third stage of validation uses
14 two SAW locations with chronosequence data. The local 0.5° DALEC calibration from the analysis was
15 used in an experiment, with 90% of woody biomass removed in the model, and regrowth followed over
16 decades using historical climate data and burned area data.

17

18 **3.3 Trendy Model Analysis**

19 18 process-based Land Surface Models (LSMs) were applied in the “Trends and Drivers of Regional Scale
20 Terrestrial Sources and Sinks of Carbon Dioxide” (Trendy-v11) project that supported the Global Carbon
21 Budget 2022 assessment (GCB2022; (Sitch et al., 2015;Friedlingstein et al., 2022)). LSMs are applied in a
22 set of factorial simulations using forcing datasets of observed global CO₂ content, observation-based
23 merged climate forcing from CRUJRA and historical Land-Use and Land cover changes (LULCC)
24 (Friedlingstein et al., 2022). For the TRENDY v11 experiments, LSMs are typically applied at 0.5-degree
25 resolution over the period 1700 to 2021. A subset of LSMs include prognostic fire models (Table S1). We
26 analysed the simulation results from the ‘S3’ simulation, where all three drivers vary, for the period 2006-
27 2017.

28 To compare data-constrained estimates of the terrestrial C cycle for the region against the Trendy ensemble,
29 we assess the agreement between domain-aggregated estimates for key C stocks and fluxes and their
30 seasonality. We also provide an indication of the spatial-temporal consistency of each LSM with our
31 CARDAMOM benchmark based on the fraction of pixels (in space and time) for which each LSM estimate
32 falls within the CARDAMOM 95% confidence interval. The outputs of the analysis are also evaluated
33 against the mean of the Trendy ensemble for the region, and against individual models using spatial



1 statistics and temporal analysis of seasonal dynamics of net exchanges (NBP) and their component
2 processes (R_a , R_h , E_{Fire}).

3

4 **3.4 Spatial carbon cycle variability and determinants**

5 The simulated C dynamics reflect the responses of the ecosystem model within a multivariate driver and
6 data space. At an individual 0.5° pixel, the model structure and retrieved parameter values determine the
7 temporal C cycle response to the environmental drivers. However, across the model domain, parameters
8 are retrieved independently for each pixel, generating an emergent map of functional variation over SAW.
9 This approach is an alternative modelling paradigm to the approach used by LSMs for which a single set
10 of model parameters is used to represent a particular plant functional type. The biogeographic gradients in
11 the C stocks and fluxes across the SAW determined by our analysis therefore represent the combination of
12 effects and interactions between the spatial variability in environmental drivers and the spatial variability
13 in ecological function, as characterised by the retrieved variations in model parameters.

14 To understand and explore the spatial sensitivity of the C cycle and ecological processes to environmental
15 factors we used a causal analysis approach similar to previous empirical studies that have synthesised
16 multiple observation streams to understand biogeographic gradients and their relationship to environmental
17 drivers (e.g. (Lehmann et al., 2014)). Common with these observation-based studies, our retrieved
18 biogeographic gradients are not determined by a prior spatial model. However, the model-data fusion
19 approach provides some key benefits, notably: (i) synthesising multiple observation streams (and
20 uncertainties) at the pixel level into an ecologically coherent and internally consistent representation of C
21 stocks and fluxes (Smallman et al., 2022), and (ii) explicitly partitioning the C dynamics along particular
22 process pathways, such as production, allocation and mortality, thus providing more detailed insights into
23 the functional variation across the SAW region.

24 We applied Wright's path approach (Runge et al., 2015; Wright, 1921, 1934) to estimate linear direct causal
25 effects that link the temporally averaged, ensemble-median C diagnostics to environmental drivers across
26 SAW. Wright's method only applies in the linear case. Here, the direct causal effect of a variable X_i on a
27 variable X_j is essentially quantified as the slope of the linear regression of X_i on X_j , where any source of
28 confounding is removed prior to the regression. Environmental drivers that we considered in the causal
29 analysis include observed meteorological variables (e.g. precipitation, abbreviated as PPTN) and modelled
30 quantities (e.g. GPP), which were selected to resolve their causal effects on C fluxes and stocks and to avoid
31 confounding. To account for the influences of climate on fire activity and productivity limitations on fuel
32 availability, we also included burned area, which was causally linked to fire-related fluxes driving mortality,
33 combustion-related emissions, and post-combustion transfers between pools. To compare linear direct
34 causal effects across variables, variables were standardised prior to the analysis. The total causal effect of



1 X_i on X_j was then estimated as the sum of the products of all possible causal pathways from X_i to X_j (Wright,
2 1934;Runge et al., 2015). Note, that when we refer to causal effects in this work, these are standardised
3 linear direct causal effects. For more detail, see the supplementary information.

4

5 4 Results

6 4.1 Calibration and validation

7 The calibration process constrained model parameters to differing degrees (Table 1). Strongest constraints
8 were for initial conditions for C pools; foliar parameters related to leaf lifespan, leaf flush and fall;
9 combustion completeness for wood; and canopy efficiency (productive capacity). The weakest constraints
10 were for residence times for litter, roots and SOM, rooting depth parameters and most fire/combustion
11 parameters. The variation in constraint is consistent with proximity of parameters to assimilated data, thus
12 parameters connected to LAI and C_{wood} are best constrained.

13 The calibrated model outputs explained much of the observed spatio-temporal variation in MODIS LAI
14 ($r^2=0.93$) and ALOS biomass ($r^2=0.99$) and the spatial variation in soil C ($r^2=0.97$). Normalised root mean
15 square errors were for LAI = 0.17; biomass = 0.06; soil C = 0.04. The calibration bias was 6% or less in all
16 cases (regression slopes: LAI =0.94; biomass=1.01; soil C =1.01).

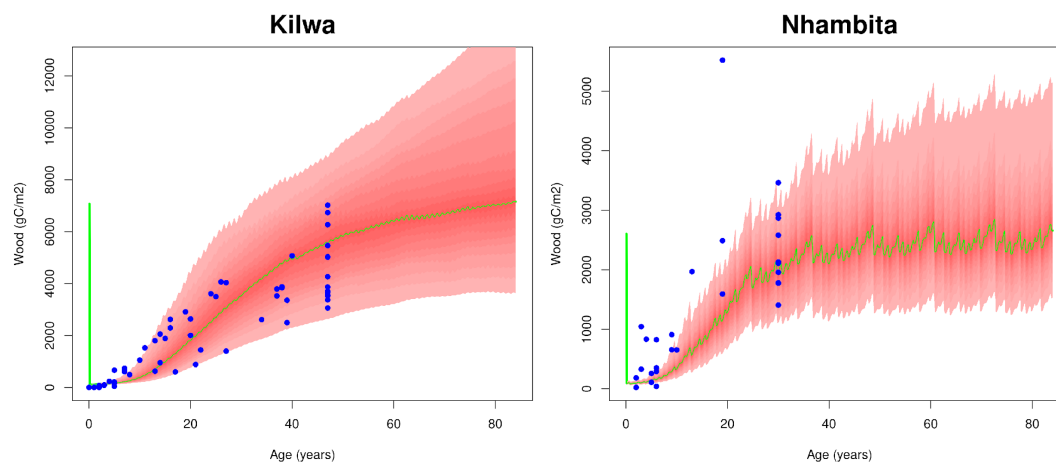
17 For NBE, CarbonTracker Europe suggests a close-to-neutral exchange, with uncertainty spanning zero
18 (Figure S 2), consistent with CARDAMOM estimates: 0.0 (95% CI -1.7-1.6) $MgC\ ha^{-1}\ y^{-1}$. CARDAMOM's
19 median regional GPP estimate was 16.1 (CI 13.1-18.8) $Mg\ C\ ha^{-1}\ yr^{-1}$, within the range of estimates from
20 the earth observation-orientated GPP products (Figure S 2). CARDAMOM's median fire emissions fell at
21 the lower end of the range of fire emissions products (Figure S 2) and its uncertainties were much larger
22 than the products' range.

23 At the locations in Mozambique and Tanzania, recovery of C_{wood} in the model was consistent with data
24 (Figure 2). The uncertainty in the model accumulation rate (95% confidence intervals) was similar in
25 magnitude to the spread of biomass across the field inventories. Differences in burned area in the model
26 simulations, rather than climate, explain the higher steady-state C_{wood} stock in the Tanzanian site.

27

28

29



1

2

3 Figure 2. Independent test of wood biomass regrowth post-disturbance at two locations in southern African
4 woodlands (left – Tanzania; right – Mozambique, note different scales). For both locations the DALEC
5 model was calibrated at quasi-steady state using local EO data over the period 2006-2017 and local data on
6 meteorology and burned area. 90% of wood steady state biomass was then removed (initial vertical green
7 line at age=0) and modelled woody biomass accumulation (green line shows median, shaded interval shows
8 95% CI) is plotted against multiple independent chronosequence estimates based on data from fallow fields
9 (blue dots).

10

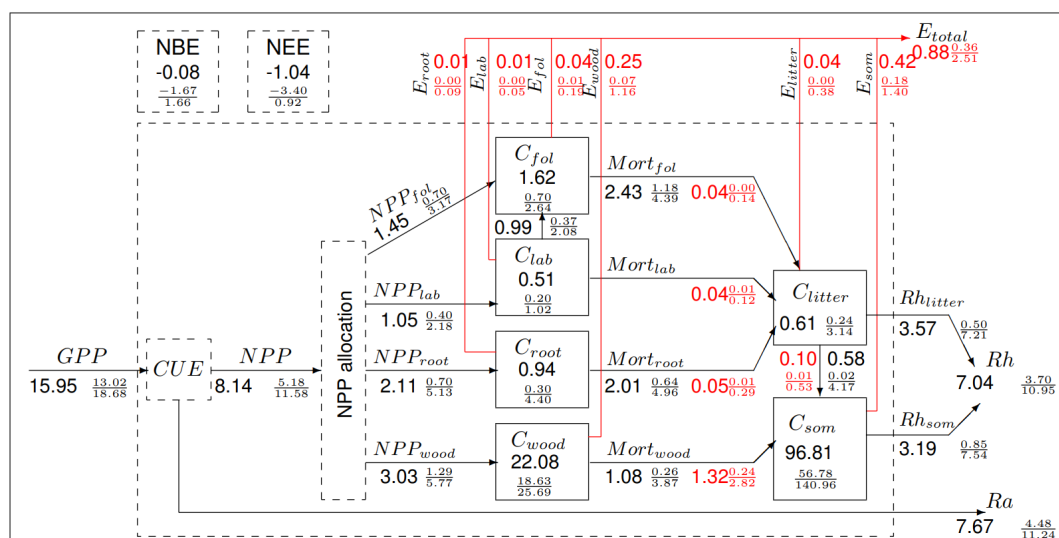
11 **4.2 The carbon cycle of the SAW region**

12 CARDAMOM estimated that 49% of regional GPP is respired (Figure 3) and remaining NPP is allocated
13 between foliage (median fraction = 0.18), a labile pool (0.13), fine roots (0.26) and C_{wood} (0.37). Each
14 ensemble member allocations sum to 1, but ensemble median fractions sum to < 1 (0.94) at the regional
15 scale because posterior distributions of allocation in the analysis are not normal.

16

17

18

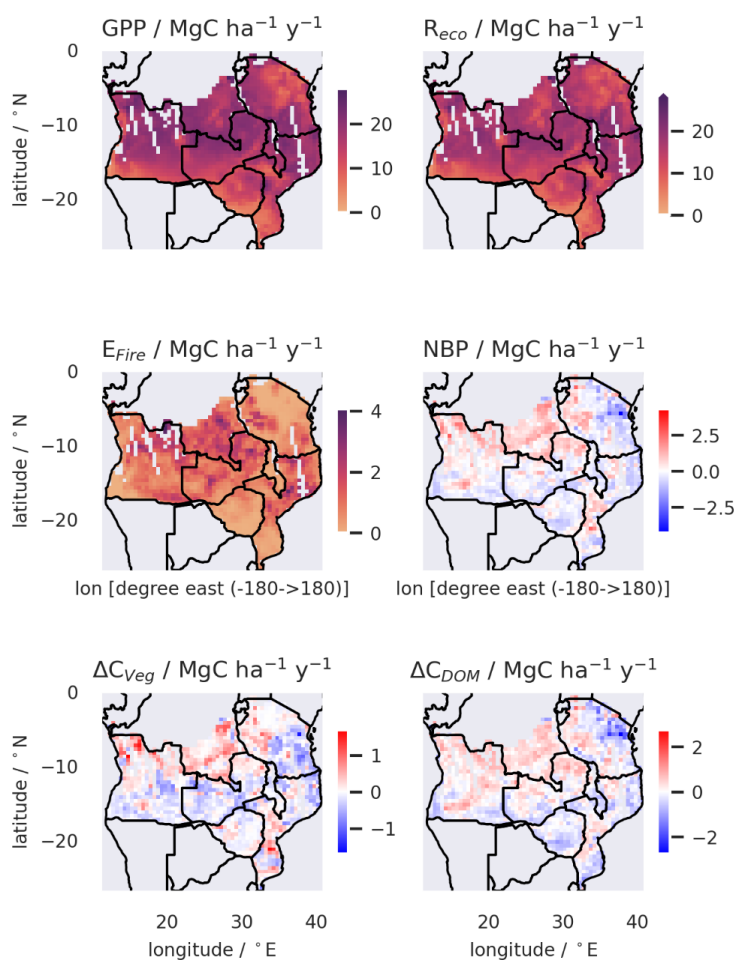


1
2 Figure 3. The C budget of the SAW region based on the CARDAMOM analysis at 0.5 x 0.5 degrees with
3 a monthly time step between 2006-2017. Numbers show estimate of fluxes (alongside arrows) and of stocks
4 (in boxes), using the mean value of all pixels in the SAW region. Units are MgC ha⁻¹ for stocks and MgC
5 ha⁻¹ yr⁻¹ for fluxes. 95% confidence intervals are shown in a fractional form with 2.5 and 97.5 percentiles
6 as numerator and denominator. Black fluxes are biogenic, including net primary production (NPP),
7 mortality (Mort), autotrophic respiration (R_a) and heterotrophic respiration (R_h). NEE = R_a+R_h–GPP. NBE
8 = NEE +E_{total}. Red disturbance fluxes are dominated by fire-driven emissions (E) and the fire-driven
9 components of plant tissue mortality or loss of litter to SOM (indicated in red figures). Note that not all
10 pools are in steady state and that the SOM pool includes coarse woody debris.

11
12 Mean residence times (MRT) of pools are sub-annual for foliage, labile, fine roots, and litter. MRT for
13 wood is 8 years (95% CI 4-20 years) and for C_{SOM} is 28 years (CI 11-90 years) (Figure S 3). Disturbance
14 fluxes are 100-fold larger from fire rather than clearance (Figure S 1). On average 23% of the region’s area
15 is burned annually, mostly set by people. Burning losses from C_{wood} are transferred to the atmosphere (~19%
16 of total disturbance flux) or to dead organic matter (~81%). Losses from the C_{wood} pool are largest through
17 fire disturbance (~59% of total mortality flux) and remaining non-fire losses encapsulate pests, diseases,
18 herbivory, plant aging, and degradation not detected by estimates of tree cover loss (Figure 3), but
19 uncertainties are large. For other pools, both live and dead, non-disturbance flux magnitudes exceed
20 disturbance fluxes. The regional C balance is approximately neutral (mean NBP: 0.0 (–1.7-1.6) Mg C ha⁻¹
21 yr⁻¹). However, in the absence of fire disturbance (i.e. NEE), the region is a potential sink of 1.0 Mg C ha⁻¹
22 yr⁻¹.



1 NBP is a function of changes to total plant biomass (sum of all live C pools, C_{veg}) and to dead organic
 2 matter (litter plus soil organic matter C, C_{DOM}), which are dominated by the two largest pools, C_{wood} and
 3 C_{SOM} . The analysis of changes to C_{veg} (ΔC_{veg}) is constrained by the assimilation of multiple biomass maps
 4 2007-2010 (Figure 4), with largest losses in the east (Tanzania and N Mozambique) and through W Zambia
 5 and S Angola. There are areas of positive ΔC_{veg} in S DRC, N Angola, E Zambia, W Zimbabwe and S
 6 Mozambique. The distribution of ΔC_{veg} is unimodal and evenly distributed between regions of increasing
 7 and decreasing C_{veg} resulting in a regionally neutral stock change for ΔC_{veg} of 0.0 (-0.4/0.43) Mg C ha⁻¹ y⁻¹
 8 ¹. The analysis of ΔC_{DOM} is not directly constrained by observations. ΔC_{DOM} is also unimodal, with a
 9 relatively even split between areas accumulating and losing C from the soil. Uncertainties on ΔC_{DOM} are
 10 approximately four times higher than for ΔC_{veg} (Figure 4).





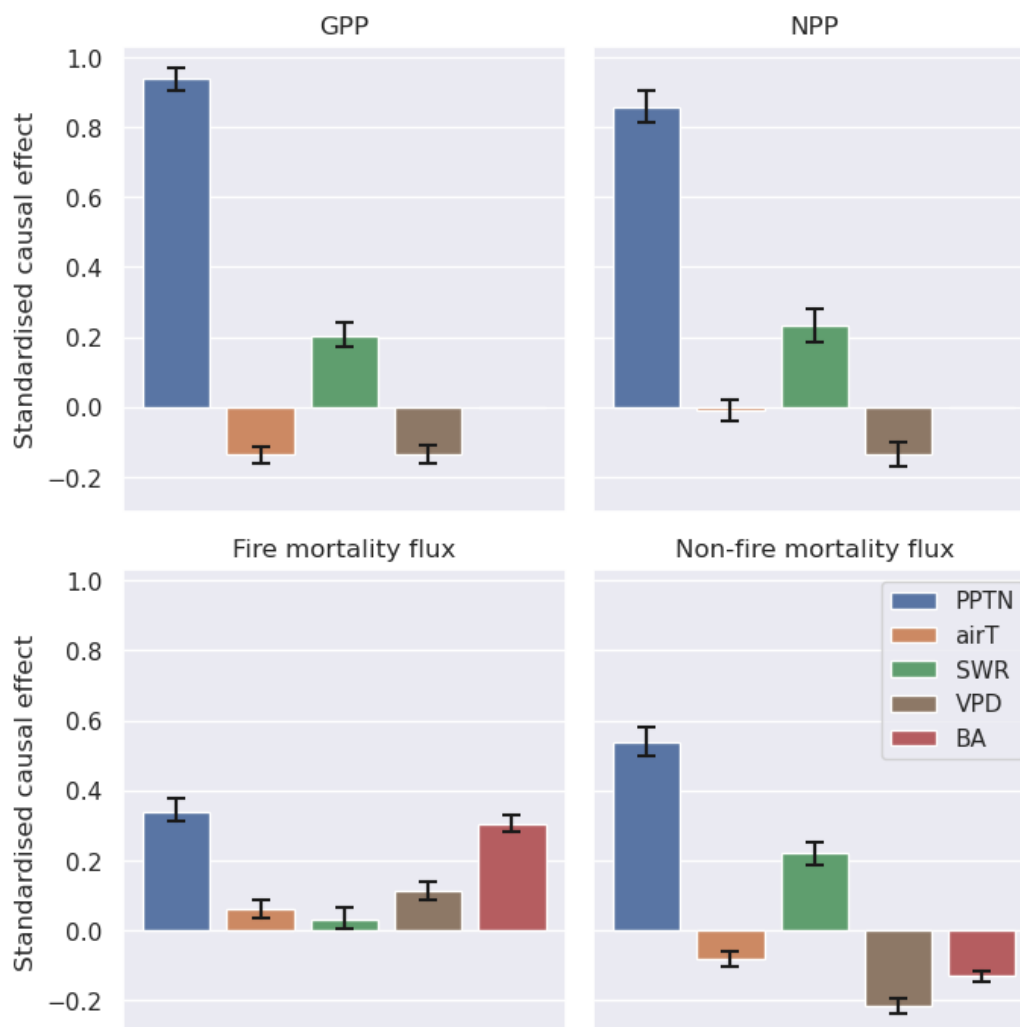
1 Figure 4. Spatial mapping of median gross fluxes, NBP, and temporally averaged rates of change in the live
2 pools ($C_{veg} = C_{wood} + C_{roots} + C_{foliage} + C_{labile}$) and dead organic matter ($C_{DOM} = C_{SOM} + C_{litter}$) C stocks across
3 the SAW region at 0.5° resolution, 2006-2017, as determined by diagnostic analysis. Gaps in maps relate
4 to areas without biomass observations due to gaps in ALOS-PALSAR data. GPP is gross primary
5 production; R_{eco} is ecosystem respiration; E_{Fire} is fire emissions; $NBP = GPP - R_{eco} - E_{Fire} -$ biomass
6 removals by management (the latter are a relatively small flux compared to the others).

7 **4.3 Environmental controls on carbon fluxes (RQ1)**

8 Median GPP distribution across the SAW region (Figure 4) is skewed unimodal, with a peak at 20 MgC ha⁻¹
9 yr⁻¹ and a tail of lower GPP (Figure S 4). R_{eco} is similarly skewed, and strongly spatially correlated ($r=0.95$)
10 with GPP, with a peak in its frequency distribution at 17 MgC ha⁻¹ yr⁻¹. Fire emissions fluxes (E_{Fire}) are
11 non-normal, dominated by low emissions (<1 MgC ha⁻¹ yr⁻¹) but with a tail of higher emissions up to 4
12 MgC ha⁻¹ yr⁻¹. The distribution of pixel-level median NBP peaks just below the source-sink boundary and
13 spans -2 to +3 MgC ha⁻¹ yr⁻¹. There is clear spatial structure to the fluxes, with higher GPP, R_{eco} , fire
14 emissions and NBP concentrated in certain areas (Figure 4) and correlated with forcings (Figure S 5).

15 The causal networks constructed to assess the controls on the spatial distribution of C fluxes identifies the
16 importance of precipitation and fire and their interactions (Figure 5, Figures S 6...S 8). Precipitation is the
17 dominant factor determining the rates of C cycling across the SAW, driving both the productivity and
18 mortality fluxes, with compensating effects on the overall C balance. Precipitation dominates the
19 distribution of GPP, with a standardised effect of 0.94 (0.90/0.98) [95% Confidence Interval]. Radiation is
20 positively linked to GPP (0.20; 0.16/0.24), while VPD (-0.13; -0.17/-0.11) and temperature are negatively
21 linked (-0.14; -0.17/-0.11). Precipitation is the dominant environmental driver of NPP (total standardised
22 effect: 0.86; 0.81/0.91), mediated by an environmental effect on carbon use efficiency (CUE). Precipitation
23 is also associated with the largest total standardised causal effects on the mortality fluxes driven by fire
24 (0.34; 0.31/0.38) and on non-fire mortality (0.55; 0.50/0.58). The total causal effect of precipitation on
25 gross fire mortality fluxes includes contributing causal pathways linked to the standing C_{veg} stocks as well
26 as through influences on the fire-driven turnover of C (Figures S 7...S 9). Fire is a key source of C losses
27 in SAW woodlands. Burned area increases along the precipitation gradient (0.43; 0.37/0.48), and with
28 increasing VPD (0.34; 0.27/0.42). Burned area drives the fire mortality flux from the C_{veg} pool (0.31;
29 0.28/0.33), with a significant mediating effect from the increasing resistance of C stocks to fire in fire-prone
30 areas described by spatial patterns in parameters (see Figure S 6).

31



1

2 Figure 5 A summary of the causal effect analysis on spatial patterns in the pixel-median estimates of key
 3 fluxes of C across the SAW region (with error bars for 95% bootstrapped CIs). Fluxes include GPP,
 4 allocation to biomass (NPP), and mortality caused by fire and non-fire factors. For each flux the
 5 standardised causal effects of different climate drivers (mean annual precipitation, PPTN; air temperature,
 6 airT; short wave radiation, SWR; vapour pressure deficit, VPD) and fire (via burned area, BA) are
 7 compared. Note that the causal analysis did not include a causal link between BA and GPP, NPP.

8

9

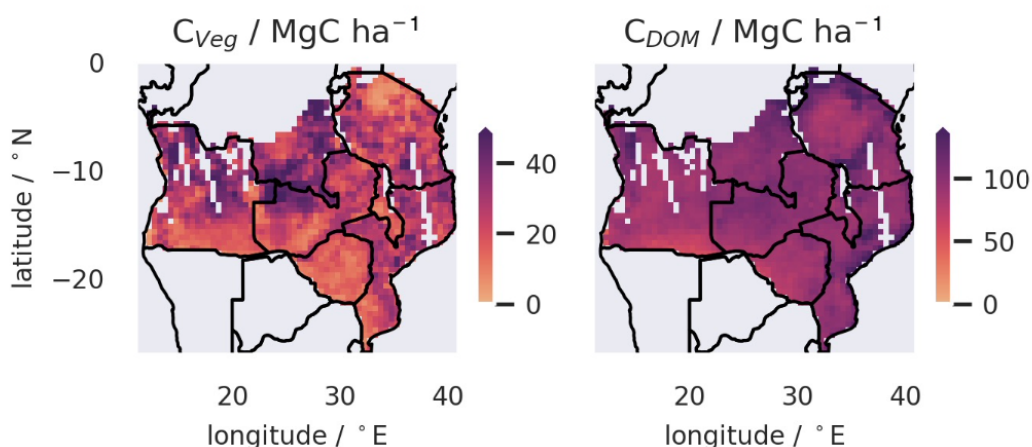


1 4.4 Environmental controls on stocks and MRT (RQ2)

2 C stocks in SAW are primarily in dead organic matter pools (C_{DOM}) with a mean of 98 MgC ha^{-1} (95%
3 confidence interval, 57-142), 99% of which is C_{SOM} to a depth of 1.0 m. Mean C_{veg} are 26 MgC ha^{-1} (22-
4 30), with 87% in C_{wood} . The mean ratio $C_{DOM}:C_{veg}$ is 4.0 (95% CI 2.1-12.5). Distributions of C stocks in live
5 and dead pools are unimodal (Figure S 9). The spatial patterns of C stocks are similar to the distributions
6 of biogenic fluxes (Figure 6).

7

8



9

10

11 Figure 6. Spatial mapping of live C stocks, which are dominated by C_{wood} (left) and dead organic C (right)
12 across the SAW region at 0.5° resolution, 2006-2017, as determined by diagnostic analysis. Gaps in maps
13 relate to areas without biomass mapping due to gaps in ALOS-PALSAR data.

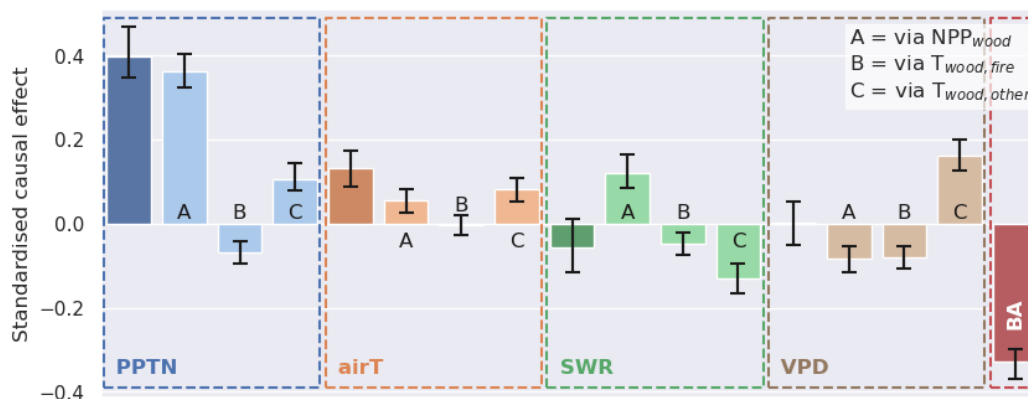
14

15 The spatial distribution of C stocks depends on C assimilated via NPP and the rate of C turnover (T) (Figures
16 7, S 6). The spatial distribution of C_{wood} is positively impacted by NPP_{wood} (standardised effect 0.65;
17 0.61/0.69) and negatively impacted by turnover rates ($T_{wood,fire}$: -0.60 ; $-0.67/-0.54$; $T_{wood,other}$: -0.54 ; $-0.58/-$
18 -0.51). Causal analysis (Figure S 6) across the spatial dataset indicates that precipitation (PPTN) impacts
19 C_{wood} along three mediating pathways: (A) positively via primary production (total effect of PPTN mediated
20 by $NPP_{wood} = 0.36$; $0.32/0.40$), (B) negatively via fire mortality rates (total effect of PPTN mediated by
21 $T_{wood,fire} = -0.07$; $-0.10/-0.04$), and (C) positively via non-fire mortality rates (total effect of PPTN mediated
22 by $T_{wood,other} = 0.11$; $0.08/0.14$). The analysis revealed clear emergent spatial variations in key functional



1 characteristics across the SAW region (Figure 8) controlling each of these pathways, including the fraction
 2 of NPP allocated to wood (A); the fire resistance of ecosystems (B, determined as biomass resilience to fire
 3 $\times (1 - \text{Combustion completeness for wood})$; see Table 1); and the non-fire median turnover rate of C_{wood} .
 4 The productivity pathway (path A) is the dominant control on the distribution of C_{wood} across the SAW
 5 (total standardised effect of PPTN on $C_{\text{wood}} = 0.40$; 0.35/0.47). The impacts on C_{wood} of turnover driven by
 6 fire ($T_{\text{wood,fire}}$) and non-fire ($T_{\text{wood,other}}$) are comparable, but opposing and spatially variable (Figure 8). In
 7 higher precipitation areas the link between relative fire mortality and burned area is weakened by a strong
 8 compensating effect of higher fire resistance of vegetation (Figure S7). The total standardised impact of
 9 fire (burned area) on C_{wood} is negative (-0.33 ; $-0.37/-0.30$). The impact of other meteorological drivers
 10 (VPD, short-wave radiation and air temperature) on C_{wood} are relatively weaker. Overall fire emissions
 11 represent a major loss from the C_{wood} pool (Figure 3), with burned area driving fire-related turnover rates
 12 (total causal effect: 0.55; 0.48/0.62) and hence MRT. We conclude that representation of SAW by a single
 13 plant functional type (PFT) approach misses important spatial functional variations in residence times and
 14 fire resistance.
 15 The turnover of the fine root and foliage C pools are dominated by the phenological turnover associated
 16 with seasonal growth and senescence directly tied to the seasonality of rainfall (Figure S7, S8). This
 17 turnover is linked to the temporally averaged meteorological drivers, although with relatively weak
 18 standardised effects. Generally, turnover rates ($1/\text{MRT}$) of both pools are negatively impacted by annual
 19 PPTN and VPD, while annual temperature and short-wave radiation (SWR) have a positive effect, although
 20 there is no clear dominant term. There is a correlation between PPTN and SWR (Pearson's $r = -0.51$).
 21 Higher MRT for roots and foliage in wetter areas suggests extended phenology both above and
 22 belowground, and identify a further important functional variation within SAW that a single PFT approach
 23 misses.

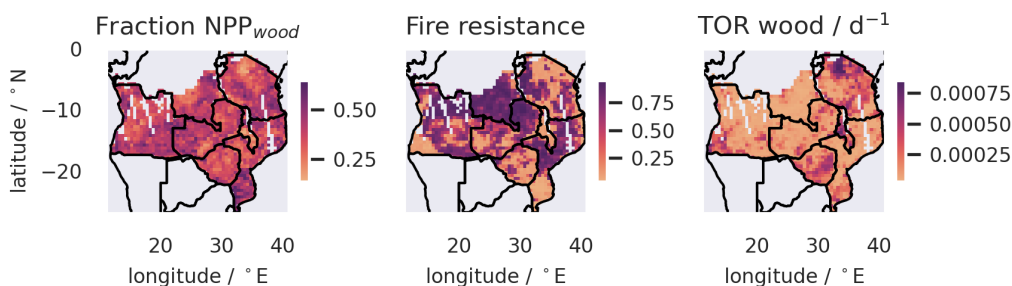
24



25



1 Figure 7 Summary of the causal effects from climate factors on spatial patterns in the pixel-median
2 estimates of total coarse wood C (C_{wood}) across the SAW region (with error bars for 95% bootstrapped CIs).
3 For mean annual precipitation (PPTN), air temperature (airT), short wave radiation (SWR), and vapour
4 pressure deficit (VPD), the total standardised causal effect is shown in the leftmost column of the four
5 panels. The three columns (A-C) show how the total effect for each factor is the outcome of three aggregated
6 causal pathways: climate effects operating through (A) changes to net primary production of wood, (B)
7 fire-driven turnover and (C) non-fire turnover. The total direct effect of fire (through burned area, BA) is
8 also shown for reference.



9

10

11 Figure 8. Spatial variations in three key ecosystem functional characteristics across Southern African
12 woodlands retrieved from the analysis. These three characteristics connect to the three pathways (Figure S
13 6) that are hypothesised to link spatial variation in environmental drivers (Figure S 1) to C_{wood} (Figure 6).
14 Pathway (A) operates via variation in woody productivity, which is a function of the fraction of total NPP
15 allocated to wood, shown in the left panel; Pathway (B) operates through C_{wood} turnover driven by fire,
16 which is linked to spatial variation in ecosystem fire resistance characteristics shown in the central panel;
17 and Pathway (C) is linked to variation in non-fire turnover rate (TOR), which has inferred spatial variations
18 as shown in the right panel.

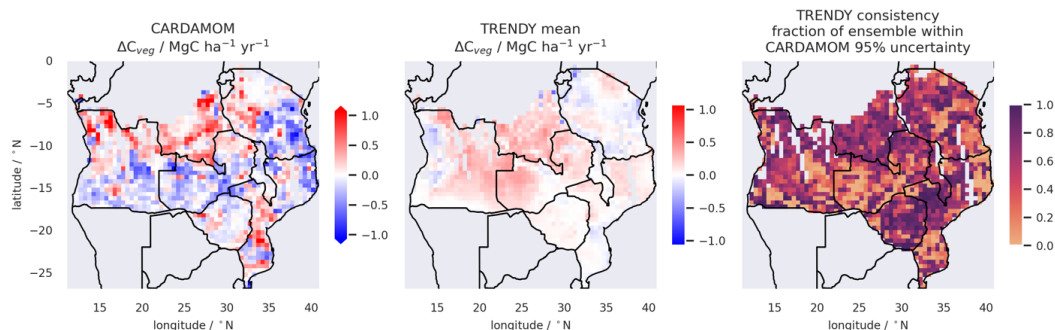
19

20 **4.5 Comparison of observation-constrained analysis of C cycling to land surface model** 21 **estimates for the SAW region (RQ3)**

22 The seasonal cycles of GPP from CARDAMOM have similar amplitude and phase to the Trendy ensemble
23 mean, but individual Trendy models had larger variations in amplitude and phase, often outside the
24 CARDAMOM confidence interval (Figure S 10). For GPP, 13 of the 18 Trendy models had regional mean



1 annual estimates within the 95% CI of CARDAMOM estimates. The median annual GPP of the Trendy
 2 ensemble ($15.8 \text{ MgC ha}^{-1} \text{ yr}^{-1}$) was 2% less than the median CARDAMOM estimate ($16.0 \text{ MgC ha}^{-1} \text{ yr}^{-1}$),
 3 and comparable to the mean estimate for GPP of the independent observation-based products for the region
 4 ($15.7 \text{ MgC ha}^{-1} \text{ yr}^{-1}$) (Figure S 2). CARDAMOM NBP amplitude was larger than all but three of the Trendy
 5 models, some of which had virtually no amplitude. These differences were linked to each major component
 6 of emissions (Figure S 11).
 7 The spatial overlap of GPP between the Trendy ensemble and CARDAMOM 95% CI was not complete,
 8 ranging from 10% to 48% (Table S2; Figure S12-13), and typically lower during each wet season. For net
 9 biome production, the mean estimates of all Trendy models were close to neutral over the region, consistent
 10 with the CARDAMOM NBP. However, there were significant differences in amplitude and spatial
 11 distribution (Table S1; Figure S13). The consistency of the spatial-temporal estimates of NBP for each
 12 LSM with the CARDAMOM 95% CI ranged from 29% to 68% (Table S2; Figure S 14-15).
 13 Estimates of C_{veg} varied markedly between Trendy LSMs ($15\text{-}66 \text{ MgC ha}^{-1}$) for the SAW region. Only three
 14 out of 18 Trendy models had regional mean C_{veg} estimates within the 95% CI of the CARDAMOM-DALEC
 15 estimates (Table S1). The spatial distribution in C_{veg} stocks varied markedly between LSMs (Figure S16-
 16 17), with spatial-temporal consistency between individual LSMs and the CARDAMOM 95% CI varying
 17 from 5% to 35% (Table S2), suggesting significant spatial biases. Considering the net change in the live
 18 vegetation pools, ΔC_{veg} , for which the CARDAMOM estimate is more closely constrained by the
 19 assimilated data than NBP, the spatially coherent discord between the Trendy LSMs and the CARDAMOM
 20 benchmark becomes more apparent (Figure 9, Figure S 17).
 21



22

23 Figure 9. A comparison the data-constrained estimate of annual mean change in vegetation C stocks (ΔC_{veg})
 24 from the CARDAMOM analysis with the mean estimate from the Trendy LSM ensemble. The right panel
 25 shows the consistency of Trendy data by mapping the fraction of the 18 ensemble members with estimates



1 within the 95% confidence interval of the CARDAMOM analysis. Data cover the SAW region and the
2 period 2006-2017.

3

4

5 5 Discussion

6 **5.1 Identification of carbon sinks and sources in the SAW region**

7 The analysis reveals a balance between sources and sinks in this region from 2006 to 2017 (Figure 4),
8 dependent on the spatial gradients in productivity, driven by precipitation, and mortality, an important
9 component of which is driven by fire (Figure 6,7). Changes in C_{veg} across the SAW have previously been
10 linked to varying patterns of land use and wood-fuel harvesting, and recovery of some woodlands with
11 reduced human pressures in other areas (McNicol et al., 2018). The explicit land-use flux modelled by
12 CARDAMOM is dependent on changes in tree cover detected by satellites, which indicated a small areal
13 extent of LUC forcing. Comparatively small disturbances typically associated with degradation processes,
14 e.g. wood-fuel harvesting, while potentially widespread (Bailis et al., 2015), are challenging to detect
15 (Milodowski et al., 2017) and maybe missed by the satellite products used in this analysis. Within the
16 CARDAMOM diagnostic analysis, C fluxes driven by non-fire degradation and not detected by GFW are
17 implicitly represented within the non-fire mortality flux, which contributes strongly to the spatial
18 distribution of ΔC_{veg} . Development and assimilation of longer time series of wood biomass with low bias,
19 alongside robust time-series estimates of degradation, extent and intensity would help to refine
20 understanding of how anthropogenic activities impact the strength of the terrestrial C sink.

21 **5.2 What are the environmental controls on exchanges of C throughout the region?**

22 The analysis supported the hypothesis that precipitation has the dominant control on GPP across the region
23 (causal effect PPTN – GPP: 0.94; 95% CI: 0.90/0.98). This strong spatial relationship was the result of (i)
24 directly modelled links between soil moisture and stomatal conductance, and (ii) correlations between LAI
25 observational data (assimilated by CARDAMOM) and patterns of precipitation. Wetter areas were thus
26 associated with moister soils and higher LAI, both stimulating higher GPP, and indicative that water
27 availability is the principal limiting factor on GPP, consistent with (limited) eddy covariance data across
28 sub-Saharan Africa (Merbold et al., 2009).

29 We expected that productivity would positively impact burned area (BA), through fuel load (Fig S 6, S 7).
30 Our results were supportive to an extent (direct standardised causal effect of NPP on BA: 0.30; 0.21/0.38)
31 (Fig S 5), but burned area was also positively related to VPD (direct causal effect of VPD on BA: 0.38;
32 0.31/0.46), indicating that climate-dependent fuel moisture limitation may be as important as fuel load. Our
33 results are consistent with assessments that identified the SAW region straddling the transition between a



1 fire regime limited by fuel build-up and one limited by fuel moisture (Archibald et al., 2009a; Alvarado et
2 al., 2020; Archibald et al., 2009b).

3 We hypothesised that NBP across SAW would be negatively impacted by the burned area fraction. The
4 analysis supported this hypothesis: burned area was a strong driver of C losses; without the contribution of
5 fire emissions, the analysis indicated that the approximately C neutral SAW would have likely been a C
6 sink. However, burned area did not drive the spatial distribution of either ΔC_{veg} or NBP, due to concurrent
7 spatial gradients in NPP driven by precipitation (Figure 5), and mediating impacts across the SAW
8 environmental gradient arising from functional variations, including changes linked to wood lifespan and
9 effective fire resistance (Figure 8). As a result, despite constituting a major driver of C losses, burned area
10 fraction is actually positively correlated in space with NBP across the region (Pearson's $r=0.28$). The
11 emergent picture from the diagnostic analysis is that the carbon balance of the SAW region is determined
12 by the interplay between precipitation-driven gradients of productivity, and losses driven by a combination
13 of fire emissions and R_h , and that these fluxes are mediated by spatial variations in plant function linked to
14 climate gradients. The finding of function-climate gradients here matches plot level analysis along
15 precipitation gradients in West Africa (Zhang-Zheng et al., 2024).

16 The coarse spatial resolution of our analysis (0.5°) is unable to resolve the fine-scale heterogeneities in the
17 landscape. Grass litter is critical fuel for fires in the region (Archibald et al., 2009b), but our analysis does
18 not separate tree and grass foliage and litter pools. Our diagnostics indicated that the fire resistance of
19 vegetation increased with burned area, but secondarily also in wetter areas. These emergent responses could
20 be explained by direct plant-level adaptation to fire (e.g. thicker bark), or through community-level
21 feedbacks where fire is excluded due to increasing tree canopy cover excluding grass (Ryan and Williams,
22 2011; Ramo et al., 2021).

23 **5.3 Controls on wood and soil C stocks**

24 We hypothesised that C stocks in soils and biomass will be spatially correlated, and their distribution
25 determined by precipitation. Our analysis was supportive, with both stocks positively and most strongly
26 driven by precipitation (total causal effect: 0.40; 0.35/0.47), despite the mediating impact of precipitation
27 on burned area. Our analysis suggests that larger C_{wood} stocks in wetter regions are sustained by a
28 combination of higher NPP and slower relative rates of turnover. Our hypothesis that C_{wood} MRT is
29 inversely related to burned area is supported by the causal analysis (Figure S 6). Fire-related mortality from
30 C_{wood} to C_{SOM} likely exceeds fire-related emissions from C_{wood} to atmosphere, and natural rates of C_{wood}
31 mortality fluxes into C_{SOM} (Figure 3). Without fire disturbance, the MRT of C_{wood} could more than double
32 from 8 to 20 years, and this would imply a similar proportional increase in steady state wood biomass,
33 increasing from a mean of 22 to 55 $MgC\ ha^{-1}$, a credible estimate based on fire exclusion experiments in
34 SAW (Ryan and Williams, 2011). Our conclusions for the dynamics of C_{SOM} are necessarily weaker. We



1 lack robust constraint on C_{SOM} dynamics, either through repeat mappings or through chronosequence studies.
2 Chronosequence data from part of the SAW suggest little change in soil C stocks after decades of post-
3 disturbance recovery.
4 We found support for our hypothesis that spatial variations in ecosystem functional characteristics influence
5 the distribution of biomass across SAW. The analysis revealed emergent regional gradients in ecosystem
6 functional characteristics related to woody allocation, wood lifespan and fire resilience (Figure 8), among
7 others. Analysis showed strong causal effects from climate and disturbance drivers on patterns of functional
8 variation (Figure S 6). Thus, wetter areas of the SAW tend to have live vegetation stocks with reduced
9 vulnerability to fire, longer wood lifespans in the absence of fire, and lower proportional allocation of NPP
10 to wood. There are also important functional variations in the dynamics of leaf and fine root pools linked
11 to climate, linked to strong phenological patterns across SAW (Ryan et al., 2017) and with impacts on
12 production patterns.

13

14 **5.4 Evaluation of Land Surface Models**

15 Our analysis supported the hypothesis that GPP and R_{eco} fluxes from the Trendy models agree more closely
16 with CARDAMOM analyses than do Trendy models' estimates of C stocks (Table S1). Nevertheless, while
17 the domain aggregate estimates for GPP were comparable between Trendy mean and CARDAMOM
18 analyses, this obscures substantial variation among models (Table S1, Table S2), which showed strong
19 spatially structured variability inconsistent with CARDAMOM estimates (Figures S14, S17) (Teckentrup
20 et al., 2021). The apparent discrepancies highlight the challenges faced by the current generation of LSMs
21 to estimates the sensitivity of GPP to soil moisture variation in water-limited environments (Paschalis et
22 al., 2020; MacBean et al., 2021). There was greater disagreement between the Trendy ensemble and the
23 CARDAMOM estimate regarding C_{veg} stock (Table S1, S2) and there were marked differences in their
24 estimates of the spatial distribution of C_{veg} (Figure S12). On average, Trendy C_{veg} across the SAW was
25 larger than CARDAMOM estimates (Table S1), in line with Trendy results over Australian savanna
26 compared with satellite estimates (Teckentrup et al., 2021) although this bias was not consistent across the
27 ensemble of LSMs.

28 Both Trendy models and CARDAMOM analyses suggest the region was close to neutral NBP. However,
29 Trendy models had lower seasonal variation in NBP than CARDAMOM. These differences were more
30 related to inconsistencies in C emissions from respiration and fire, rather than foliar phenology and GPP.
31 The low amplitude of NBP in Trendy models results from a strong temporal coupling in GPP and R_{eco} .
32 CARDAMOM analyses have large seasonal amplitudes arising from seasonal divergence, due to litter
33 production occurring at the end of the wet season, leading to dry season decomposition, coupled also with
34 dry season fires. The DALEC model lacks a soil moisture control on R_h , whereas most Trendy models do



1 include this relation. This structural difference may explain temporal differences in R_h (Fig S 11),
2 particularly as the assimilated data have no direct constraint on R_h .

3

4 **5.5 Conclusions**

5 Our analysis reveals that carbon dynamics of the SAW are determined by the interplay between
6 precipitation and fire, mediated by substantial spatial variations in plant functional characteristics. Spatial
7 analyses from model-data fusion provided insights into SAW C dynamics variation in response to the
8 regional gradients in climate and disturbance. Precipitation is the dominant control on both primary
9 productivity (GPP) and C residence times. GPP variations are controlled directly by precipitation, through
10 soil moisture limitation on primary production, and indirectly through functional variations in phenology
11 (LAI). Precipitation gradients impact C residence times indirectly, through correlated variations in related
12 functional characteristics. For instance, precipitation is linked to patterns of effective fire resistance in
13 vegetation, and to variation in lifespan of C_{wood} when fire is absent (Figure 8). Consequently, the spatial
14 distribution of C stocks across the SAW is significantly determined by the precipitation gradient through
15 multiple interacting pathways.

16 The full C cycle analysis of the region is the current state-of-the art due to its direct incorporation of repeat
17 biomass maps that are locally calibrated and validated. The analysis suggests that C_{wood} mortality driven by
18 fire is attributed as the major loss term from C_{wood} , albeit with large uncertainties (Figure 3). The fire-driven
19 fall in C_{wood} residence time across the precipitation gradient linked to rising burned area and fire mortality
20 (Figure 5), acts to damp positive feedbacks between increasing GPP and C_{wood} . If fire effects are removed,
21 our analysis suggest a ~3-fold increase in C_{wood} (Bond et al., 2005). Much larger uncertainties remain in the
22 analysis of soil C due to sparsity of data compared to aboveground biomass.

23 This analysis has mapped variation in functional characteristics, challenging the use of a single PFT for this
24 region. CARDAMOM suggests substantial variations in functional characteristics across the SAW, for
25 instance for wood, foliar and fine root lifespans and allocation, and fire resistance. These variations likely
26 explain why LSM estimates are inconsistent with the data-constrained estimates from this study. Individual
27 LSMs deviated inconsistently from CARDAMOM estimates, with individual components of the C cycle
28 varying in space and between models. C_{veg} stocks and fire emissions were the source of largest discrepancy,
29 alongside the temporal distribution of fluxes.

30 The C budgets here can also support more robust and observationally consistent national reporting in the
31 region for the Paris Agreement of the UNFCCC. The detailed resolution of the outputs, with locally valid
32 functional characteristics, can enhance national CO₂ emission factors for fire disturbance, for instance.
33 Working closely with national agencies, approaches such as demonstrated could deliver Tier 3 estimates of
34 national C budgets to support countries world-wide.



1

2 6 Acknowledgements

3 We thank Ben Poulter and Anthony Walker for their comments on the manuscript. We recognise UKRI
4 grants to SEOSAW (NE/P008755/1), SECO (NE/T01279X/1), and NCEO. C Roesch and GH also thank
5 the European Union's Horizon 2020 research and innovation programme under Marie Skłodowska-Curie
6 grant agreement No. 860100 (iMIRACLI). We acknowledge and thank the broader CARDAMOM
7 developer team. We thank the data providers from the Trendy LSM teams, MODIS teams, and SoilGrids
8 community. C Ryan and IMM would like to thank JAXA for support via the EO-RA3 agreement no.
9 ER3A2N035. The authors declare no conflicts of interest. This research was funded in whole, or in part, by
10 NERC grants NE/P008755/1 and NE/T01279X/1. For the purpose of open access, the author has applied a
11 creative commons attribution (CC BY) licence to any author accepted manuscript version arising.

12

13

14 7. Data Availability

15 The data that support the findings of this study are available in a resource at
16 <https://doi.org/10.7488/ds/7776>. “Williams, Mathew; Milodowski, David Thomas; Smallman, Thomas
17 Luke. (2024). Monthly Net Biome Exchange for the Southern African Woodlands 2006-2017 estimated
18 using the CARDAMOM model-data fusion framework, 2006-2017. University of Edinburgh”.

19

20 8. Author Contribution

21 MW, DTM and TLS conceived the analysis with support from CMRy, KGD and SS. DTM and TLS
22 developed the model code and undertook the analysis with support from CMRo and GGH, and IMM, MOS
23 and AV. DTM, TLS and MW produced visualisations. MW supervised the research and wrote the
24 manuscript with input from all authors. MW, CMRy, KGD and SS provided funding for the work.

25

26 9. Competing Interests

27 The authors declare that they have no conflict of interest.

28

29 References

30 Alvarado, S. T., Andela, N., Silva, T. S., and Archibald, S.: Thresholds of fire response to moisture and
31 fuel load differ between tropical savannas and grasslands across continents, *Global Ecology and*
32 *Biogeography*, 29, 331-344, 2020.



- 1 Andela, N., Morton, D. C., Giglio, L., Chen, Y., van der Werf, G. R., Kasibhatla, P. S., DeFries, R. S.,
2 Collatz, G. J., Hantson, S., Kloster, S., Bachelet, D., Forrest, M., Lasslop, G., Li, F., Mangeon, S.,
3 Melton, J. R., Yue, C., and Randerson, J. T.: A human-driven decline in global burned area, *Science*,
4 356, 1356-1362, doi:10.1126/science.aal4108, 2017.
- 5 Archibald, S., Kirton, A., Merwe, M. v. d., Scholes, R. J., Williams, C. A., and Hanan, N.: Drivers of
6 interannual variability in Net Ecosystem Exchange in a semi-arid savanna ecosystem, *South Africa*,
7 *Biogeosciences*, 6, 251-266, 2009a.
- 8 Archibald, S., Roy, D. P., Van Wilgen, B. W., and Scholes, R. J.: What limits fire? An examination of
9 drivers of burnt area in Southern Africa, *Global Change Biology*, 15, 613-630,
10 <https://doi.org/10.1111/j.1365-2486.2008.01754.x>, 2009b.
- 11 Archibald, S., Lehmann, C. E. R., Gómez-Dans, J. L., and Bradstock, R. A.: Defining pyromes and global
12 syndromes of fire regimes, *Proceedings of the National Academy of Sciences*, 110, 6442-6447,
13 10.1073/pnas.1211466110, 2013.
- 14 Bailis, R., Drigo, R., Ghilardi, A., and Masera, O.: The carbon footprint of traditional woodfuels, *Nature*
15 *Climate Change*, 5, 266-272, 2015.
- 16 Bloom, A. A., and Williams, M.: Constraining ecosystem carbon dynamics in a data-limited world:
17 integrating ecological "common sense" in a model-data-fusion framework, *Biogeosciences*, 12, 1299-
18 1315., 10.5194/bg-11-12733-2014, 2015.
- 19 Bloom, A. B., Exbrayat, J.-F., Velde, I. R. v. d., Feng, L., and Williams, M.: The decadal state of the
20 terrestrial carbon cycle: global retrievals of terrestrial carbon allocation, pools and residence times,
21 *Proceedings of the National Academy of Sciences*, 113, 1285-1290, 2016.
- 22 Bond, W. J., Woodward, F. I., and Midgley, G. F.: The global distribution of ecosystems in a world
23 without fire, *New Phytologist*, 165, 525-538, doi:10.1111/j.1469-8137.2004.01252.x, 2005.
- 24 Campbell, B. M.: *The Miombo in transition : woodlands and welfare in Africa*, Center for International
25 Forestry Research, Bogor, Indonesia, 1996.
- 26 Chidumayo, E.: Changes in miombo woodland structure under different land tenure and use systems in
27 central Zambia, *Journal of Biogeography*, 29, 1619-1626, 2002.
- 28 Chidumayo, E.: Forest degradation and recovery in a miombo woodland landscape in Zambia: 22 years of
29 observations on permanent sample plots, *Forest Ecology and Management*, 291, 154-161, 2013.
- 30 Chidumayo, E. N.: Development of *Brachystegia-Julbernardia* woodland after clear-felling in central
31 Zambia: Evidence for high resilience, *Applied Vegetation Science*, 7, 237-242, 2004.
- 32 Chuvieco, E., Mouillot, F., Van der Werf, G. R., San Miguel, J., Tanase, M., Koutsias, N., García, M.,
33 Yebra, M., Padilla, M., and Gitas, I.: Historical background and current developments for mapping
34 burned area from satellite Earth observation, *Remote Sensing of Environment*, 225, 45-64, 2019.
- 35 Ciaais, P., Bombelli, A., Williams, M., Piao, S. L., Chave, J., Ryan, C. M., Henry, M., Brender, P., and
36 Valentini, R.: The Carbon balance of Africa: Synthesis of Recent Research Studies, *Phil. Trans. R.*
37 *Soc. A.*, 369, 2038-2057, 2011.
- 38 Collalti, A., and Prentice, I.: Is NPP proportional to GPP? Waring's hypothesis 20 years on, *Tree*
39 *physiology*, 39, 1473-1483, 2019.
- 40 Dexter, K., Smart, B., Baldauf, C., Baker, T., Balinga, M., Brienen, R., Fauset, S., Feldpausch, T., Silva,
41 L., and Muledi, J. I.: Floristics and biogeography of vegetation in seasonally dry tropical regions,
42 *International Forestry Review*, 17, 10-32, 2015.
- 43 Ernst, Y., Archibald, S., Balzter, H., Chevallier, F., Ciaais, P., Fischer, C. G., Gaubert, B., Higginbottom,
44 T., Higgins, S., Lawal, S., Lacroix, F., Lauerwald, R., Lourenco, M., Martens, C., Mengistu, A. G.,
45 Merbold, L., Mitchard, E., Moyo, M., Nguyen, H., O'Sullivan, M., Rodríguez-Veiga, P., Rosan, T.,
46 Rosentreter, J., Ryan, C., Scheiter, S., Sitch, S., Stevens, N., Tagesson, T., Tian, H., Wang, M.,
47 Woon, J. S., Zheng, B., Zhou, Y., and Scholes, R. J.: The African Regional Greenhouse Gases
48 Budget (2010–2019), *Global Biogeochemical Cycles*, 38, e2023GB008016,
49 <https://doi.org/10.1029/2023GB008016>, 2024.



- 1 Exbrayat, J. F., Smallman, T. L., Bloom, A. A., Hutley, L. B., and Williams, M.: Inverse determination of
2 the influence of fire on vegetation carbon turnover in the pantropics, *Global Biogeochemical Cycles*,
3 32, 1776-1789, 2018.
- 4 Fawcett, D., Cunliffe, A. M., Sitch, S., O'sullivan, M., Anderson, K., Brazier, R. E., Hill, T. C., Anthoni,
5 P., Arneth, A., and Arora, V. K.: Assessing model predictions of carbon dynamics in global drylands,
6 *Frontiers in Environmental Science*, 10, 790200, 2022.
- 7 Friedlingstein, P., O'Sullivan, M., Jones, M. W., Andrew, R. M., Gregor, L., Hauck, J., Le Quéré, C.,
8 Lujikx, I. T., Olsen, A., Peters, G. P., Peters, W., Pongratz, J., Schwingshackl, C., Sitch, S., Canadell,
9 J. G., Ciais, P., Jackson, R. B., Alin, S. R., Alkama, R., Arneth, A., Arora, V. K., Bates, N. R.,
10 Becker, M., Bellouin, N., Bittig, H. C., Bopp, L., Chevallier, F., Chini, L. P., Cronin, M., Evans, W.,
11 Falk, S., Feely, R. A., Gasser, T., Gehlen, M., Gkritzalis, T., Gloege, L., Grassi, G., Gruber, N.,
12 Gürses, Ö., Harris, I., Hefner, M., Houghton, R. A., Hurtt, G. C., Iida, Y., Ilyina, T., Jain, A. K.,
13 Jersild, A., Kadono, K., Kato, E., Kennedy, D., Klein Goldewijk, K., Knauer, J., Korsbakken, J. I.,
14 Landschützer, P., Lefèvre, N., Lindsay, K., Liu, J., Liu, Z., Marland, G., Mayot, N., McGrath, M. J.,
15 Metzl, N., Monacci, N. M., Munro, D. R., Nakaoka, S. I., Niwa, Y., O'Brien, K., Ono, T., Palmer, P.
16 I., Pan, N., Pierrot, D., Pockock, K., Poulter, B., Resplandy, L., Robertson, E., Rödenbeck, C.,
17 Rodriguez, C., Rosan, T. M., Schwinger, J., Séférian, R., Shutler, J. D., Skjelvan, I., Steinhoff, T.,
18 Sun, Q., Sutton, A. J., Sweeney, C., Takao, S., Tanhua, T., Tans, P. P., Tian, X., Tian, H., Tilbrook,
19 B., Tsujino, H., Tubiello, F., van der Werf, G. R., Walker, A. P., Wanninkhof, R., Whitehead, C.,
20 Willstrand Wranne, A., Wright, R., Yuan, W., Yue, C., Yue, X., Zaehle, S., Zeng, J., and Zheng, B.:
21 Global Carbon Budget 2022, *Earth Syst. Sci. Data*, 14, 4811-4900, 10.5194/essd-14-4811-2022,
22 2022.
- 23 Friend, A. D., Lucht, W., Rademacher, T. T., Kerbin, R., Betts, R., Cadule, P., Ciais, P., Clark, D. B.,
24 Dankers, R., and Falloon, P. D.: Carbon residence time dominates uncertainty in terrestrial vegetation
25 responses to future climate and atmospheric CO₂, *Proceedings of the National Academy of Sciences*,
26 111, 3280-3285, 2014.
- 27 Fuster, B., Sánchez-Zapero, J., Camacho, F., García-Santos, V., Verger, A., Lacaze, R., Weiss, M., Baret,
28 F., and Smets, B.: Quality assessment of PROBA-V LAI, fAPAR and fCOVER collection 300 m
29 products of copernicus global land service, *Remote Sensing*, 12, 1017, 2020.
- 30 Giglio, L., Boschetti, L., Roy, D. P., Humber, M. L., and Justice, C. O.: The Collection 6 MODIS burned
31 area mapping algorithm and product, *Remote Sensing of Environment*, 217, 72-85,
32 <https://doi.org/10.1016/j.rse.2018.08.005>, 2018.
- 33 Godlee, J. L., Ryan, C. M., Bauman, D., Bowers, S. J., Carreiras, J. M., Chisingui, A. V., Cromsigt, J. P.,
34 Druce, D. J., Finckh, M., and Gonçalves, F. M.: Structural diversity and tree density drives variation
35 in the biodiversity–ecosystem function relationship of woodlands and savannas, *New Phytologist*,
36 232, 579-594, 2021.
- 37 Gonçalves, F. M., Revermann, R., Gomes, A. L., Aidar, M. P., Finckh, M., and Juergens, N.: Tree species
38 diversity and composition of Miombo woodlands in South-Central Angola: A chronosequence of
39 forest recovery after shifting cultivation, *International Journal of Forestry Research*, 2017, 6202093,
40 2017.
- 41 Hansen, M. C., Potapov, P. V., Moore, R., Hancher, M., Turubanova, S. A., Tyukavina, A., Thau, D.,
42 Stehman, S. V., Goetz, S. J., Loveland, T. R., Kommareddy, A., Egorov, A., Chini, L., Justice, C. O.,
43 and Townsend, J. R. G.: High-Resolution Global Maps of 21st-Century Forest Cover Change,
44 *Science*, 342, 850-853, 10.1126/science.1244693, 2013.
- 45 Harris, I. C.: CRU JRA v1.1: A forcings dataset of gridded land surface blend of Climatic Research Unit
46 (CRU) and Japanese reanalysis (JRA) data; Jan.1901 - Dec.2017, Centre for Environmental Data
47 Analysis, 2019.
- 48 Hengl, T., Mendes de Jesus, J., Heuvelink, G. B., Ruiperez Gonzalez, M., Kilibarda, M., Blagotić, A.,
49 Shangquan, W., Wright, M. N., Geng, X., and Bauer-Marschallinger, B.: SoilGrids250m: Global
50 gridded soil information based on machine learning, *PLoS one*, 12, e0169748, 2017.



- 1 Joiner, J., and Yoshida, Y.: Global MODIS and FLUXNET-derived Daily Gross Primary Production,
2 V2<https://doi.org/10.3334/ORNLDAAC/1835>, 2021.
- 3 Jung, M., Schwalm, C., Migliavacca, M., Walther, S., Camps-Valls, G., Koirala, S., Anthoni, P., Besnard,
4 S., Bodesheim, P., Carvalhais, N., Chevallier, F., Gans, F., Goll, D. S., Haverd, V., Köhler, P., Ichii,
5 K., Jain, A. K., Liu, J., Lombardozzi, D., Nabel, J. E. M. S., Nelson, J. A., O'Sullivan, M., Pallandt,
6 M., Papale, D., Peters, W., Pongratz, J., Rödenbeck, C., Sitch, S., Tramontana, G., Walker, A.,
7 Weber, U., and Reichstein, M.: Scaling carbon fluxes from eddy covariance sites to globe: synthesis
8 and evaluation of the FLUXCOM approach, *Biogeosciences*, 17, 1343-1365, 10.5194/bg-17-1343-
9 2020, 2020.
- 10 Kaiser, J., Heil, A., Andreae, M., Benedetti, A., Chubarova, N., Jones, L., Morcrette, J.-J., Razinger, M.,
11 Schultz, M., and Suttie, M.: Biomass burning emissions estimated with a global fire assimilation
12 system based on observed fire radiative power, *Biogeosciences*, 9, 527-554, 2012.
- 13 Kalaba, F. K., Quinn, C. H., Dougill, A. J., and Vinya, R.: Floristic composition, species diversity and
14 carbon storage in charcoal and agriculture fallows and management implications in Miombo
15 woodlands of Zambia, *Forest Ecology and Management*, 304, 99-109, 2013.
- 16 Kattge, J., Diaz, S., Lavorel, S., Prentice, I., Leadley, P., Bönisch, G., Garnier, E., Westoby, M., Reich, P.
17 B., and Wright, I.: TRY—a global database of plant traits, *Global Change Biology*, 17, 2905-2935,
18 2011.
- 19 Koren, G.: Constraining the exchange of carbon dioxide over the Amazon: New insights from stable
20 isotopes, remote sensing and inverse modeling, PhD thesis, Wageningen, the Netherlands,,
21 Wageningen University, 2020.
- 22 Lehmann, C. E. R., Anderson, T. M., Sankaran, M., Higgins, S. I., Archibald, S., Hoffmann, W. A.,
23 Hanan, N. P., Williams, R. J., Fensham, R. J., Felfili, J., Hutley, L. B., Ratnam, J., San Jose, J.,
24 Montes, R., Franklin, D., Russell-Smith, J., Ryan, C. M., Durigan, G., Hiernaux, P., Haidar, R.,
25 Bowman, D. M. J. S., and Bond, W. J.: Savanna Vegetation-Fire-Climate Relationships Differ
26 Among Continents, *Science*, 343, 548-552, 10.1126/science.1247355, 2014.
- 27 Levick, S. R., Baldeck, C. A., and Asner, G. P.: Demographic legacies of fire history in an African
28 savanna, *Functional Ecology*, 29, 131-139, <https://doi.org/10.1111/1365-2435.12306>, 2015.
- 29 MacBean, N., Scott, R. L., Biederman, J. A., Peylin, P., Kolb, T., Litvak, M. E., Krishnan, P., Meyers, T.
30 P., Arora, V. K., Bastrikov, V., Goll, D., Lombardozzi, D. L., Nabel, J. E. M. S., Pongratz, J., Sitch,
31 S., Walker, A. P., Zaehle, S., and Moore, D. J. P.: Dynamic global vegetation models underestimate
32 net CO₂ flux mean and inter-annual variability in dryland ecosystems, *Environmental Research*
33 *Letters*, 16, 094023, 10.1088/1748-9326/ac1a38, 2021.
- 34 McNicol, I. M., Ryan, C. M., and Williams, M.: How resilient are African woodlands to disturbance from
35 shifting cultivation?, *Ecological Applications*, 25, 2320--2336, 10.1890/14-2165.1.sm, 2015.
- 36 McNicol, I. M., Ryan, C. M., and Mitchard, E. T.: Carbon losses from deforestation and widespread
37 degradation offset by extensive growth in African woodlands, *Nature communications*, 9, 1-11, 2018.
- 38 McNicol, I. M., Keane, A., Burgess, N. D., Bowers, S. J., Mitchard, E. T., and Ryan, C. M.: Protected
39 areas reduce deforestation and degradation and enhance woody growth across African woodlands,
40 *Communications Earth & Environment*, 4, 392, 2023.
- 41 Merbold, L., Ardö, J., Arneth, A., Scholes, R. J., Nouvellon, Y., Grandcourt, A. d., Archibald, S.,
42 Bonnefond, J. M., Boulain, N., Bruemmer, C., Brueggemann, N., Cappelaere, B., Ceschia, E., El-
43 Khidir, H. A. M., El-Tahir, B. A., Falk, U., Lloyd, J., Kergoat, L., Dantec, V. L., Mougín, E.,
44 Muchinda, M., Mukelabai, M. M., Ramier, D., Rouspard, O., Timouk, F., Veenendaal, E. M., and
45 Kutsch, W. L.: Precipitation as driver of carbon fluxes in 11 African ecosystems, *Biogeosciences*, 6,
46 1027–1041, 2009.
- 47 Milodowski, D., Mitchard, E., and Williams, M.: Forest loss maps from regional satellite monitoring
48 systematically underestimate deforestation in two rapidly changing parts of the Amazon,
49 *Environmental Research Letters*, 12, 094003, 2017.
- 50 Mistry, J.: *World Savannas*, Routledge, Abingdon, UK, 2014.



- 1 Mitchard, E. T. A., Saatchi, S. S., Woodhouse, I. H., Nangendo, G., S.Ribeiro, N., Williams, M., Ryan, C.
2 M., Lewis, S. L., Feldpausch, T. R., and Meir, P.: Using satellite radar backscatter to predict above-
3 ground woody biomass: A consistent relationship across four different African landscapes, *Geophys.*
4 *Res. Lett.*, 36, L23401, 2009.
- 5 Moncrieff, G. R., Scheiter, S., Bond, W. J., and Higgins, S. I.: Increasing atmospheric CO₂ overrides the
6 historical legacy of multiple stable biome states in Africa, *New Phytologist*, 201, 908-915,
7 <https://doi.org/10.1111/nph.12551>, 2014.
- 8 Myneni, R., Knyazikhin, Y., and Park, T.: MODIS/Terra+Aqua Leaf Area Index/FPAR 8-Day L4 Global
9 500m SIN Grid V061 [Data set]., NASA <https://doi.org/10.5067/MODIS/MCD15A2H.061>, 2021.
- 10 Osborne, C. P., Charles-Dominique, T., Stevens, N., Bond, W. J., Midgley, G., and Lehmann, C. E. R.:
11 Human impacts in African savannas are mediated by plant functional traits, *New Phytologist*, 220,
12 10-24, <https://doi.org/10.1111/nph.15236>, 2018.
- 13 Paschalis, A., Fatichi, S., Zscheischler, J., Ciais, P., Bahn, M., Boysen, L., Chang, J., De Kauwe, M.,
14 Estiarte, M., Goll, D., Hanson, P. J., Harper, A. B., Hou, E., Kigel, J., Knapp, A. K., Larsen, K. S.,
15 Li, W., Lienert, S., Luo, Y., Meir, P., Nabel, J. E. M. S., Ogaya, R., Parolari, A. J., Peng, C.,
16 Peñuelas, J., Pongratz, J., Rambal, S., Schmidt, I. K., Shi, H., Sternberg, M., Tian, H., Tschumi, E.,
17 Ukkola, A., Vicca, S., Viovy, N., Wang, Y.-P., Wang, Z., Williams, K., Wu, D., and Zhu, Q.:
18 Rainfall manipulation experiments as simulated by terrestrial biosphere models: Where do we stand?,
19 *Global Change Biology*, 26, 3336–3355, [10.1111/gcb.15024](https://doi.org/10.1111/gcb.15024), 2020.
- 20 Pennington, R. T., Lehmann, C. E., and Rowland, L. M.: Tropical savannas and dry forests, *Current*
21 *Biology*, 28, R541-R545, 2018.
- 22 Ramo, R., Roteta, E., Bistinas, I., Van Wees, D., Bastarrika, A., Chuvieco, E., and Van der Werf, G. R.:
23 African burned area and fire carbon emissions are strongly impacted by small fires undetected by
24 coarse resolution satellite data, *Proceedings of the National Academy of Sciences*, 118,
25 e2011160118, 2021.
- 26 Ribeiro, N. S., Katerere, Y., Chirwa, P. W., and Grundy, I. M.: Miombo woodlands in a changing
27 environment: Securing the resilience and sustainability of people and woodlands, *Springer Nature*,
28 2020.
- 29 Runge, J., Petoukhov, V., Donges, J. F., Hlinka, J., Jajcay, N., Vejmelka, M., Hartman, D., Marwan, N.,
30 Paluš, M., and Kurths, J.: Identifying causal gateways and mediators in complex spatio-temporal
31 systems, *Nature communications*, 6, 8502, 2015.
- 32 Ryan, C., and Williams, M.: How does fire intensity and frequency affect miombo woodland tree
33 populations and biomass?, *Ecological Applications*, 21, 48-60, 2011.
- 34 Ryan, C. M., Williams, M., and Grace, J.: Above and Below Ground Carbon Stocks in a Miombo
35 Woodland Landscape of Mozambique, *Biotropica*, 43, 423-432, 2011.
- 36 Ryan, C. M., Hill, T. C., Woollen, E., Ghee, C., Mitchard, E. T. A., Cassells, G., Grace, J., Woodhouse, I.
37 H., and Williams, M.: Quantifying small-scale deforestation and forest degradation in African
38 woodlands using radar imagery, *Global Change Biology*, 18, 243-257, 2012.
- 39 Ryan, C. M., Williams, M., Hill, T. C., Grace, J., and Woodhouse, I. H.: Assessing the phenology of
40 southern tropical Africa: A comparison of hemispherical photography, scatterometry, and
41 optical/NIR remote sensing, *IEEE Transactions on Geoscience and Remote Sensing*, 52, 519-528,
42 [10.1109/TGRS.2013.2242081](https://doi.org/10.1109/TGRS.2013.2242081), 2014.
- 43 Ryan, C. M., Pritchard, R., McNicol, I., Owen, M., Fisher, J. A., and Lehmann, C.: Ecosystem services
44 from southern African woodlands and their future under global change, *Philosophical Transactions of*
45 *the Royal Society B: Biological Sciences*, 371, 20150312, 2016.
- 46 Ryan, C. M., Williams, M., Grace, J., Woollen, E., and Lehmann, C. E. R.: Pre-rain green-up is
47 ubiquitous across southern tropical Africa: implications for temporal niche separation and model
48 representation, *New Phytologist*, 213, 625-633, <https://doi.org/10.1111/nph.14262>, 2017.
- 49 Sankaran, M., Hanan, N. P., Scholes, R. J., Ratnam, J., Augustine, D. J., Cade, B. S., Gignoux, J.,
50 Higgins, S. I., Le Roux, X., Ludwig, F., Ardo, J., Banyikwa, F., Bronn, A., Bucini, G., Caylor, K. K.,
51 Coughenour, M. B., Diouf, A., Ekaya, W., Feral, C. J., February, E. C., Frost, P. G. H., Hiernaux, P.,



- 1 Hrabar, H., Metzger, K. L., Prins, H. H. T., Ringrose, S., Sea, W., Tews, J., Worden, J., and
2 Zambatis, N.: Determinants of woody cover in African savannas, *Nature*, 438, 846-849, 2005.
- 3 SEOSAW partnership: A network to understand the changing socio-ecology of the southern African
4 woodlands (SEOSAW): Challenges, benefits, and methods, *Plants, People, Planet*, 3, 249-267, 2021.
- 5 Sitch, S., Friedlingstein, P., Gruber, N., Jones, S. D., Murray-Tortarolo, G., Ahlström, A., Doney, S. C.,
6 Graven, H., Heinze, C., and Huntingford, C.: Recent trends and drivers of regional sources and sinks
7 of carbon dioxide, *Biogeosciences*, 12, 653-679, 2015.
- 8 Smallman, T. L., and Williams, M.: Description and validation of an intermediate complexity model for
9 ecosystem photosynthesis and evapotranspiration: ACM-GPP-ETv1, *Geosci. Model Dev.*, 12, 2227-
10 2253, 10.5194/gmd-12-2227-2019, 2019.
- 11 Smallman, T. L., Milodowski, D. T., Neto, E. S., Koren, G., Ometto, J., and Williams, M.: Parameter
12 uncertainty dominates C cycle forecast errors over most of Brazil for the 21st Century, *Earth System
13 Dynamics*, 12, 1191–1237, 10.5194/esd-2021-17, 2021.
- 14 Smallman, T. L., Milodowski, D. T., and Williams, M.: From Ecosystem Observation to Environmental
15 Decision-Making: Model-Data Fusion as an Operational Tool, *Frontiers in Forests and Global
16 Change*, 4, 818661, 2022.
- 17 Teckentrup, L., De Kauwe, M. G., Pitman, A. J., Goll, D. S., Haverd, V., Jain, A. K., Joetzjer, E., Kato,
18 E., Lienert, S., Lombardozzi, D., McGuire, P. C., Melton, J. R., Nabel, J. E. M. S., Pongratz, J., Sitch,
19 S., Walker, A. P., and Zaehle, S.: Assessing the representation of the Australian carbon cycle in
20 global vegetation models, *Biogeosciences*, 18, 5639-5668, 10.5194/bg-18-5639-2021, 2021.
- 21 van der Werf, G. R., Randerson, J. T., Giglio, L., van Leeuwen, T. T., Chen, Y., Rogers, B. M., Mu, M.,
22 van Marle, M. J. E., Morton, D. C., Collatz, G. J., Yokelson, R. J., and Kasibhatla, P. S.: Global fire
23 emissions estimates during 1997–2016, *Earth Syst. Sci. Data*, 9, 697-720, 10.5194/essd-9-697-2017,
24 2017.
- 25 Waring, R. H., Landsberg, J. J., and Williams, M.: Net primary production of forests: a constant fraction
26 of gross primary production?, *Tree Physiology*, 18, 129-134, 1998.
- 27 Williams, M., Schwarz, P., Law, B. E., Irvine, J., and Kurpius, M. R.: An improved analysis of forest
28 carbon dynamics using data assimilation, *Global Change Biology*, 11, 89-105, 2005.
- 29 Williams, M., Ryan, C. M., Rees, R. M., Sambane, E., Fernando, J., and Grace, J.: Carbon sequestration
30 and biodiversity of re-growing miombo woodlands in Mozambique, *Forest Ecology and
31 Management*, 254, 145-155, 2008.
- 32 Wright, S.: Correlation and causation, *Journal of agricultural research*, 20, 557, 1921.
- 33 Wright, S.: The method of path coefficients, *The annals of mathematical statistics*, 5, 161-215, 1934.
- 34 Yin, Y., Bloom, A. A., Worden, J., Saatchi, S., Yang, Y., Williams, M., Liu, J., Jiang, Z., Worden, H.,
35 Bowman, K., Frankenberg, C., and Schimel, D.: Fire decline in dry tropical ecosystems enhances
36 decadal land carbon sink, *Nature Communications*, 11, 1900, 10.1038/s41467-020-15852-2, 2020.
- 37 Zhang-Zheng, H., Adu-Bredu, S., Duah-Gyamfi, A., Moore, S., Addo-Danso, S. D., Amissah, L.,
38 Valentini, R., Djagbletey, G., Anim-Adjei, K., Quansah, J., Sarpong, B., Owusu-Afryie, K.,
39 Gvozdevaite, A., Tang, M., Ruiz-Jaen, M. C., Ibrahim, F., Girardin, C. A. J., Rifai, S., Dahlsjö, C. A.
40 L., Riutta, T., Deng, X., Sun, Y., Prentice, I. C., Oliveras Menor, I., and Malhi, Y.: Contrasting
41 carbon cycle along tropical forest aridity gradients in West Africa and Amazonia, *Nature
42 Communications*, 15, 3158, 10.1038/s41467-024-47202-x, 2024.
- 43
44